Self-assembly of Li single-ion-conducting block copolymers for improved conductivity and viscoelastic properties

Self-assembly of Li single-ion-conducting block copolymers for improved conductivity and viscoelastic properties

Elena I. Lozinskaya[a,*], Denis O. Ponkratov[a], Inna A. Malyshkina[b], Patrick Grysan[c], Gabriele Lingua[d,e], Claudio Gerbaldi[d,e,*], Alexander S. Shaplov[c,*] and Yakov S. Vygodskii[a]

[a] *A.N. Nesmeyanov Institute of Organoelement Compounds Russian Academy of Sciences (INEOS RAS), Vavilov str. 28, 119991 Moscow, GSP-1, Russia*

[b] *Moscow State University (MSU), Department of Physics, Vorob'evy gory, 119992, Moscow, Russia*

[c] *Luxembourg Institute of Science and Technology (LIST), 5 avenue des Hauts-Fourneaux, L-4362 Esch-sur-Alzette, Luxembourg*

[d] *GAME Lab, Department of Applied Science and Technology (DISAT), Politecnico di Torino, Corso Duca degli Abruzzi 24, 10129, Torino, Italy*

[e] *National Reference Center for Electrochemical Energy Storage (GISEL) - INSTM, Via G. Giusti 9, 50121, Firenze, Italy*

ABSTRACT

Single-ion conducting polyelectrolytes (SICPs) with mobile Li cation have recently gathered significant attention as an "ideal" electrolyte for safe solid-state rechargeable lithium batteries, because they eliminate salt concentration gradients and concentration overpotentials, allowing transference number (t_{Li+}) values close to unity. In this work, a series of single ion conducting block copolymers, namely [$(LiM)_n$-*r*-$(PEGM)_m$]-*b*-$(PhEtM)_k$ (A-*b*-B), is synthesized via reversible addition-fragmentation chain transfer (RAFT) copolymerization of 1-[3-(methacryloyloxy)propylsulfonyl]-(trifluoromethanesulfonyl)imide (LiM), poly(ethylene glycol)methyl ether methacrylate (PEGM) and 2-phenylethyl methacrylate (PhEtM) with controlled PEGM:LiM ratio, molecular weights (M_n=25.8 ÷ 85.9 kDa) and narrow polydispersity (M_w/M_n=1.12 ÷ 1.21). The bulk ionic conductivity, solid-state morphology and thermal properties of block copolymers are studied as a function of their composition. Block copolymers

[*]Corresponding authors. Tel.: +7 499 7025870, E-mail address: helloz@ineos.ac.ru (E.I. Lozinskaya); Tel.: +352 275 888 4579, E-mail address: alexander.shaplov@list.lu (A.S. Shaplov); Tel.: +39 011 090 4643, E-mail address: claudio.gerbaldi@polito.it (C. Gerbaldi).

having molecular weights in the range of 46 ÷ 63 kDa and any ratio of PEGM:LiM (from 3:1 to 7:1) tend to evolve in quasi-hexagonally-packed cylinders, while copolymers with higher molecular weights (M_n > 74 kDa) and the ratio of PEGM:LiM = 5:1 and $M_A/M_B \leq 2.0$ show lamellar phase separation. The lamellar long-range ordering in poly[(LiM_{17}-*r*-$PEGM_{86}$)-*b*-$PhEtM_{131}$] and poly[(LiM_{17}-*r*-$PEGM_{86}$)-*b*-$PhEtM_{194}$] results not only in the improved viscoelastic (mechanical) performance compared to parent copolymer poly[LiM_{17}-*r*-$PEGM_{86}$] (complex viscosity = 2.5×10^8 mPa s and 8.7×10^4 mPa s at 25 °C, respectively), but also in the demonstration of sufficiently high ionic conductivity despite the decrease in Li^+ amount ($\sigma = 3.8\times10^{-7}$ and 4.1×10^{-7} S/cm at 25 °C, correspondingly). The selected poly[(LiM_{17}-*r*-$PEGM_{86}$)-*b*-$PhEtM_{131}$] further shows high t_{Li+} (0.96 at 70°C) and wide electrochemical stability (4.4 V *vs.* Li^+/Li at 70°C), which results in reversible and stable cycling at high specific capacities (up to 150 and 118 mAh g^{-1} at C/20 and C/5 rates, respectively) when assembled in lab-scale truly-solid-state Li metal cells with Li/copolymer/$LiFePO_4$ configuration.

Keywords: single-ion conductor, poly(ionic liquid), polyelectrolyte, ionic conductivity, Li battery

1. Introduction

The global growth in the production of portable digital devices, drones and electric vehicles demands the development of low-cost, high-performance and reliable batteries with improved cycle life [1–5]. Lithium-ion batteries (LiBs) are the key commercial technology due to the high energy density, lightweight, fast charge/discharge, and long lifetime. However, the performance of standard LiBs with non-aqueous liquid electrolytes cannot satisfy the practical requirement of next-generation, high-demanding applications, due to the relatively high reactivity and intrinsic instability of liquid electrolytes especially at the electrode/electrolyte interface [6–8]. Moreover, the application of Li metal as anode material results in additional safety problems, that include uncontrolled growth of dendrites, relatively infinite volume expansion and an unfavorable solid electrolyte interphase (SEI) formation caused by the high reactivity of lithium metal [9]. Finally, any significant temperature (overheating during high power use) or voltage

(overcharge) variations lead to the battery instability, namely to gas evolution, depressurization of the battery case, catching fire, etc. [9].

The need for safe and reliable Li batteries inspires the research on innovative electrolyte materials. Solid polymer electrolytes (SPEs), representing solid solutions of alkali metal salts in polymers, were proposed for batteries in 1973 because they combine the advantages of solid-state electrochemistry with the ease of processing inherent to plastic materials [10]. SPEs offer high thermal stability, non-volatility, high electrochemical stability and prevent the risk of electrolyte leaks outside the battery case [11]. Notwithstanding all of the advantages, SPEs suffer from the joint mobility of both cations and anions, thus creating concentration gradients (polarization) and dendrite growth at the surface of metal Li anode [12]. The alternative approach to salt-in-polymer SPEs is to incorporate covalently bonded lithium salt moieties into the main polymer chain. Such polymers, being constructed of a main polymer chain with fixed anionic functional groups and lithium ions as the mobile counterpart, are termed single-ion Li-conducting polymers (SICPs) [13,14]. A number of SICPs representing various linear and crosslinked systems, random and block copolymers and having different attached anions were published in recent years [13–37]. However, the majority of them failed to show significant superiority over SPEs until the introduction of highly delocalized anions attributable to ionic liquids [13,38]. Later, a novel class of SICPs, namely anionic poly(ionic liquid)s with Li counterions, demonstrated the following advantages over conventional dual-ion conducting SPEs: enhanced chemical/electrochemical stabilities, absence of concentration gradients and unity Li transference numbers [39].

In general, the ideal SICP for a solid-state battery should have the ionic conductivity of a liquid (>10^{-5} S/cm at 25^{o}C), the mechanical properties of a solid, and the formability of a commodity thermoplastic [40]. However, the reciprocal association between high bulk ionic conductivity and low T_g has limited the simultaneous realization of high toughness, flexibility and electrochemical performance in a single-component linear SICP [41]. One of the approaches to overcome this problem was firstly demonstrated by Elabd and Winey et al. [42–46] and consisted in the synthesis of cationic block copolymers, where the partial incompatibility between ionic and neutral blocks resulted in a microphase-separated morphology. Block copolymers based on methyl methacrylate and 1-[(2-methacryloyloxy)ethyl]-3-butylimidazolium bis(trifluoromethanesulfonyl)

imide showed two orders of magnitude higher ionic conductivity than random copolymers having similar composition [42]. Moreover, at comparable polyelectrolyte composition, the poly[(styrene)-*b*-(1-((2-acryloyloxy)ethyl)-3-butylimidazolium bis(trifluoromethanesulfonyl)imide)] block copolymer with strong microphase separation exhibited ~1.5-2 orders of magnitude higher ionic conductivity than poly[(MMA)-*b*-(1-[(2-methacryloyloxy)ethyl]-3-butylimidazolium bis(trifluoromethanesulfonyl)imide)] block copolymer with weak microphase separation [43]. Such effect was explained by the existence of a correlation between the morphology of block copolymers and their ionic conductivity. As a result of strong microphase segregation, the nanoscale domains were formed, thus playing the role of ion-conducting channels with elevated concentration of mobile ions and enhanced conductivity [43]. In addition, the orientation of conducting microdomains and the interaction between polymer backbone and ionic moiety of charged block were significantly affecting the ionic conductivity. The efficiency of charge transport in cationic polyionic liquids (PILs) was increasing with the transition from hexagonally packed cylinders (1-D conducting pathway), lamellae (2-D conducting pathway) to 3-D network structures (continuous conducting microdomain) [43]. Later, Bailey et al. [47] studied the phase behavior of block copolymers obtained by ring-opening metathesis polymerization (ROMP) from norbornene monomers, namely neutral bicyclo[2.2.1]hept-5-ene-2-carboxylic acid dodecyl ester and ionic 3-bicyclo[2.2.1]hept-5-en-2-ylmethyl-1-hexyl-3H-imidazolium bis(trifluoromethanesulfonyl)imide. The obtained cationic block architectures produced each of the classic equilibrium morphologies including lamellae, hexagonally packed cylinders, and spheres on a body-centered cubic lattice [47]. It is important to mention that all samples demonstrated excellent preservation of structural order over a wide range of temperatures, which is extremely important for the future application of such functional materials.

In spite of the set of publications dedicated to the phase separation in cationic block copolymers, only a few reports examined the relationship between morphological behavior and ion transport in anionic SICPs with lithium counter ion [25,28,48–51]. All reported block copolymers had different architectures (A-B diblock [48–50], B-A-B triblock [25,51], C-AB-C triblock copolymers [28] (Scheme 1)), but they were mainly synthesized from one ionic monomer, namely from lithium 4-styrene sulphonyl(trifluoromethanesulphonyl) imide (LiSTFSI). Balsara and coworkers [48,49]

synthesized poly[(ethylene oxide)-*b*-(LiSTFSI)] (A-B) diblock copolymers, where the molecular weight of the PEO block was fixed at 5000 g/mol, while the M_n of LiSTFSI block was varied from 2000 to 7500 g/mol. (Scheme 1, **1**). At temperatures below melting of the PEO block (T_m<50°C), the copolymers with molecular weights of LiSTFSI block ≤ 4000 g/mol exhibited lamellar microphase separation with crystalline PEO-rich microphases and ionic clusters in the glassy LiSTFSI-rich microphases. As Li ions were trapped in such clusters, the ionic conductivity was very low (10^{-9}-10^{-8} S/cm at 25°C). An increase in temperature above 60°C led to a transition from an ordered structure to a homogeneous disordered morphology, where the Li ions were released from the clusters, which correspondingly increased the ionic conductivity by five orders of magnitude (up to 10^{-4}÷10^{-3} S/cm at 60°C). Similar temperature dependence of ionic conductivity was observed in poly[(LiSTFSI)-*b*-(ethylene oxide)-*b*-(LiSTFSI)] (B-A-B) triblock copolymers developed by Bouchet and Armand et al. (Scheme 1, **2**) [25,51]. The significant increase of conductivity was detected with the transition from lamellar microphase separation to the disordered morphology at temperatures above the melting point of PEO block (*T*>55°C). In contrast, Long and co-workers used a different strategy forming triblock copolymers (C-AB-C), where the central block was not composed solely by poly(LiSTFSI), but rather by random copolymerization of LiSTFSI with di(ethylene glycol) methyl ether methacrylate (Scheme 1, **4**) [28]. Such an approach featured a microphase-separated morphology and a combination of excellent mechanical properties and high ion transport. It was shown that when the ion density in the central block was increased in 2.7 times, the ion conductivity increased almost 3 orders of magnitude (up to 1.3×10^{-6} S/cm at 25°C). The authors explained this effective ion transfer not only by an increase in the number of lithium cations, but also by a substantial improvement in microphase segregation (lamellar period - 24.2 nm) and channel connectivity [28]. These results can be explained as follows: the mechanism of Li ion transfer in PEO derived materials is based on hopping of the Li between oxygen atoms in oxy ethylene units. When PEO chains are "frozen" and separated from LiSTFSI block in lamellar morphology, the Li ions are trapped and cannot move. Thus, polymers **1**, **2** and **3** (Scheme 1) do not benefit from the phase separation, and ionic conductivity starts to increase only when block copolymers become a disordered system. However, when in triblock copolymer the LiSTFSI is copolymerized randomly in the middle block with a monomer

having short and flexible side PEO chains (Scheme 1, **4**), such system still allows for Li hopping, while also profiting an improved mechanical performance from lamellar microphase separation.

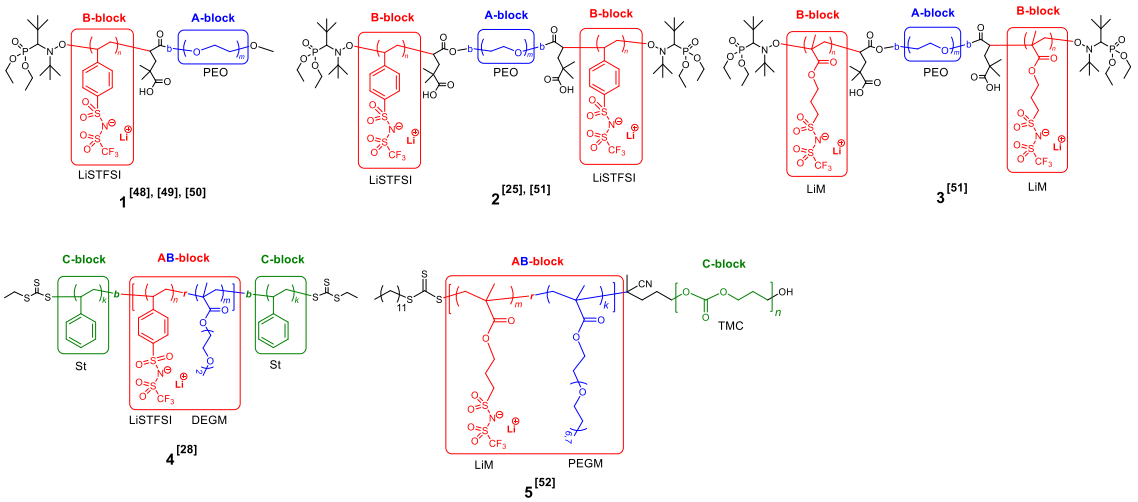

Scheme 1. An overview of the anionic single ion conducting block copolymers reported in literature (**1** to **5**, including references to the related articles).

Recently, we reported the preparation of anionic single-ion conducting block copolymers via a combination of the ring opening polymerization (ROP) of trimethylene carbonate (TMC) monomer and subsequent RAFT copolymerization of lithium 1-[3-(methacryloyloxy)propylsulfonyl]-1-(trifluoromethylsulfonyl)imide and poly(ethylene glycol) methyl ether methacrylate (PEGM) [52]. The obtained poly[TMC_n-*b*-(LiM_m-*r*-$PEGM)_k$] block copolymers (Scheme 1, **5**) evolved in a quasi-hexagonally-packed cylinders morphology and demonstrated improved viscoelastic properties, along with an outstanding stability vs. anodic oxidation (exceeding 4.8 V vs. Li^+/Li at 70°C) in comparison with parent poly[LiM_m-*r*-$PEGM_k$]. Moreover, while it was possible to gain the control over the molecular weight of [LiM_m-*r*-$PEGM_k$] block and the LiM:PEGM ratio, the molar mass of TMC block was fixed to 20000 g/mol due to the limitations of the ROP method. However, the ionic conductivity of poly[TMC_n-*b*-(LiM_m-*r*-$PEGM)_k$] was still two times lower than that of poly[LiM_m-*r*-$PEGM_k$] .

The objective of this work is to successfully demonstrate the synthesis of a set of novel A-B block copolymers with single Li-ion conducting features, where A block represents a random copolymer of LiM and PEGM, while B block consists of poly(2-

phenylethyl methacrylate) (poly(PhEtM), Scheme 2) and to investigate the impact of microphase segregation on ionic conductivity and mechanical properties of the resultant polyelectrolytes. Moreover, as poly[(LiM$_n$-*r*-PEGM$_m$)-*b*-PhEtM$_k$] block copolymers were prepared solely by RAFT method, this allowed the manage not only the LiM:PEGM ratio, but also the molecular weights of both blocks, thus gaining the control over the microphase separation as well. The best block copolymers, namely poly[(LiM$_{17}$-*r*-PEGM$_{86}$)-*b*-PhEtM$_{131}$] and poly[(LiM$_{17}$-*r*-PEGM$_{86}$)-*b*-PhEtM$_{194}$], afforded lamellar microphase separation and demonstrated significantly improved viscoelastic properties (3 to 5 orders of magnitude increase in storage moduli, at both 25 and 70°C) at similar level of ionic conductivity in comparison with random poly[LiM$_{17}$-*r*-PEGM$_{86}$]. Finally, poly[(LiM$_{17}$-*r*-PEGM$_{86}$)-*b*-PhEtM$_{131}$] having high lithium-ion transference number and high oxidative stability, was used for the assembly of lab-scale Li-metal cell prototypes, which showed reversible cycling near theoretical capacity, thus demonstrating the promising prospects of the new single-ion conductors for the development of truly solid-state lithium polymer batteries.

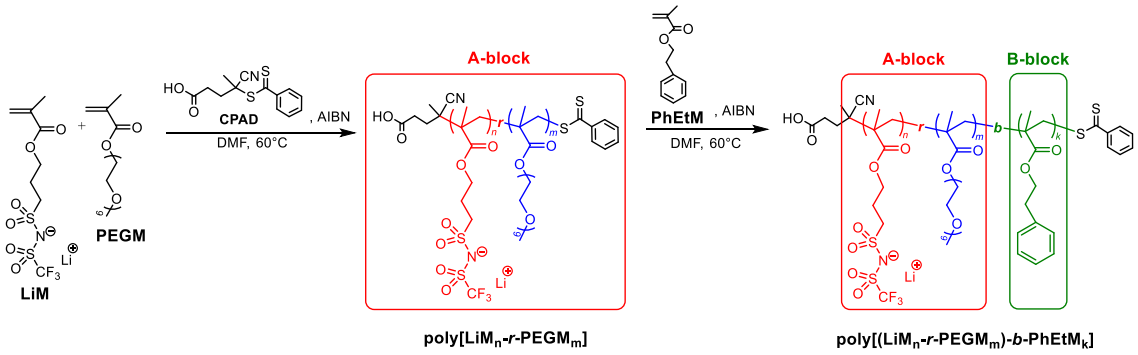

Scheme 2. Poly[(LiM$_\mathbf{n}$-*r*-PEGM$_m$)-*b*-PhEtM$_\mathbf{k}$] block copolymers prepared in this work via RAFT copolymerization.

2. Experimental

2.1 Materials

Poly(ethylene glycol)methyl ether methacrylate (PEGM, M_n=500 g/mol, Aldrich), 2-phenylethyl methacrylate (PhEtM, 98%, Jinan Yudong Technology Co., Ltd), dimethylformamide (DMF, HPLC grade 99.5%, Acros), lithium bis(trifluoromethanesulfonyl)imide (LiTFSI, 99%, Acros), 4-cyano-4-(phenylcarbonothioylthio)pentanoic acid (CPAD, >97%, Aldrich), 4-methoxyphenol

(99%, Acros), 1-methyl-2-pyrrolidinone (NMP, 99.5% anhydrous, Acros), carbon-coated lithium iron phosphate ($LiFePO_4$, LFP, Advanced Lithium Electrochemistry Co. Ltd.), carbon black C_{65} (Timcal) and lithium metal foil (high purity lithium metal, Albemarle) were used as received, without further purification. Diethyl ether (Et_2O, 99%) was distilled over Na. 2,2'-Azobisisobutyronitrile (AIBN, initiator, 98%, Aldrich) was recrystallized from methanol. The Spectra/Por 1 (Spectrum labs) dialysis tubing with MWCO 6000-8000 Dalton was used for polymer dialysis.

2.2 Synthesis of LiM and copolymers

The lithium 1-[3-(methacryloyloxy)propylsulfonyl]-1-(trifluoromethanesulfonyl)imide (LiM) ionic monomer was synthesized in full accordance with the procedure published previously [33]. The resulting crystalline powder was dried at 25 °C/1 mm Hg overnight and stored under inert atmosphere in an argon-filled glove-box (MBRAUN MB-Labstar, H_2O and O_2 content < 0.5 ppm). Spectroscopic data of the target compound were in full accordance with those reported in the literature [33,52].

Random copolymers poly[LiM_n-*r*-$PEGM_m$] were prepared via RAFT copolymerization of LiM and PEGM monomers. Then, the poly[(LiM_n-*r*-$PEGM_m$) was directly used as macro-CTA for the RAFT synthesis of block poly[(LiM_n-r-$PEGM_m$)-b-$PhEtM_k$] copolymers. For the detailed copolymerization procedure please refer to the supporting information (loadings for the synthesis of poly[LiM_n-*r*-$PEGM_m$] and poly[(LiM_n-r-$PEGM_m$)-b-$PhEtM_k$] copolymers are presented in Table S1 and Table S3 respectively).

Indeed, the kinetics of PhEtM RAFT polymerization was studied by an example of CPAD to monomer ratio, set to target a molecular weight ($M_{n\ theo}$) of 19.7 kDa (poly$(PhEtM)_{103}$); full details in the supporting information.

2.3 Characterization

2.3.1 Physico-chemical characterization

NMR spectra were recorded on AMX-400 spectrometer (Bruker, Germany) at 25°C in the indicated deuterated solvent and are listed in ppm. The signal corresponding to the residual protons of the deuterated solvent was used as an internal standard for ^{1}H and ^{13}C

NMR, while for ^{19}F NMR the $CHCl_2F$ was utilized as an external standard. IR spectra were acquired on a Nicolet Magna-750 Fourier IR-spectrometer using ATR technology (128 scans, resolution is 2 cm^{-1}).

The number-average molecular weights ($M_{n(SEC)}$) and M_w/M_n ratios for copolymers were determined by size exclusion chromatography (SEC) on a LC-20AD gel permeation chromatograph (GPC, Shimadzu Corporation) equipped with PLgel 5μm MIXED-D column (Agilent Technologies), PLgel 5μm (Agilent Technologies) pre-column and a refractive index detector (RID-20A, Shimadzu Corporation). The system was operated at 50°C and 1.0 mL/min flow using 0.1 M $Li(CF_3SO_2)_2N$ solution in DMF as an eluent. Poly(methyl methacrylate) standards (EasiVial PM, Agilent Technologies, M_p = 550 - 1558×10^3) were used to perform calibration.

The $M_{n(NMR)}$ for random poly[LiM_n-*r*-$PEGM_m$] copolymers was defined using simplified equation 1:

$$M_{n(NMR)} = \overline{M}_{unit} \cdot q \cdot \frac{[LiM]_0+[PEGM]_0}{[CPAD]_0} + M_{CPAD} \qquad (1),$$

where q is the total conversion of PEGM and LiM monomers (determined by ^1H NMR); M_{CPAD} is the molar mass of CPAD; $[PEGM]_o$, $[LiM]_o$ and $[CPAD]_o$ are the initial amount of monomers and CPAD in moles; $\overline{M}_{unit}$ - the average molecular weight of the monomer repeating unit, which is calculated in accordance with equation (2):

$$\overline{M}_{unit} = \frac{n}{n+m} \cdot M_{LiM} + \frac{m}{n+m} \cdot M_{PEGM} \quad (2),$$

where $n=q\cdot[LiM]_o$, $m=q\cdot[PEGM]_o$, M_{LiM} and M_{PEGM} are the molar masses of the respective monomers.

The $M_{n(NMR)}$ for block poly[(LiM_n-r-$PEGM_m$)-b-$PhEtM_k$] copolymers was calculated by simplified equation (3):

$$M_{n(NMR)} = M_{PhEtM} \cdot q \cdot \frac{[PhEtM]_0}{[macro-CTA]_0} + M_{macro-CTA} \qquad (3),$$

where q is the conversion of PhEtM monomer (determined by ^1H NMR); $M_{macro\text{-}CTA}$ – the molecular weight of respective macro-CTA poly[LiM_n-*r*-$PEGM_m$] determined by ^1H NMR (see section 2.6.3.); M_{PhEtM} is the molar mass of PhEtM; $[PhEtM]_o$ and [macro-$CTA]_o$ are the initial amounts of monomer and macro-CTA, respectively. The number of monomer units k in poly[(LiM_n-r-$PEGM_m$)-b-$PhEtM_k$] was calculating as follows: $k= q\cdot[PhEtM]_o$.

AFM images were recorded with MFP-3D infinity microscope (Asylum Instruments/Oxford Instruments) in the tapping mode with the Heater-Cooler environmental option (-20°C, under nitrogen atmosphere). AC160TS-R3 (Olympus) cantilevers were applied with a stiffness of 26 N m^{-1} and resonance frequency of 300 KHz. The images were recorded in the so-called 'soft tapping mode', to avoid deformation and indentation of the polymer surface by the tip. All the images were collected with the maximum available number of pixels (512) in each direction. The domains periodicity was evaluated on averaged Power Density Spectrum (PSD) generated from phase shift channel on 3 different 500 x 500 nm^2 images. General procedure for the preparation of the samples for AFM was as follow: films were cast from 10 wt% solution of respective block copolymer in DMF on a microscope glass, and allowed to slowly evaporate at 80°C. The obtained thin films were dried at 80°C/1 mm Hg for 24 h. Prior to AFM analysis, sample were soaked in anhydrous ethanol for a few seconds and then was dried under a nitrogen flux.

Thermal mechanical analysis (TMA) of block copolymers samples was performed under inert atmosphere (He) using a DIL 402 select Expedis dilatometer (NETZSCH, Selb, Germany) at a heating rate of 5 °C min^{-1} and a constant load of 0.3 N. Heat distortion temperature (T_{HDT}) was determined as a temperature at which a noticeable deformation under applied load and scanning/heating rate was observed.

Differential scanning calorimetry (DSC) was performed on a DSC 204 F1 Phoenix instrument (NETZSCH, Germany) in the range of -70-150°C at a heating rate of 5°C min^{-1} under argon atmosphere. Three heating-cooling cycles were carried out for each sample. Glass transition temperatures (T_g) were calculated using Proteus 6.1 software and the reported values obtained as an average from the second and third heating curves.

Rheology measurements were performed using an Anton Paar Physica MCR 302 rheometer equipped with a CTD 450 temperature control device with a disposable aluminum plate-plate (diameter: 25 mm, measure gap: 1 mm) geometry. Poly[(LiM_{17}-*r*-$PEGM_{86}$)-*b*-$PhEtM_{131}$] and poly[LiM_{17}-r-$PEGM_{86}$] samples were loaded directly onto the aluminum plate of the rheometer and special care was taken to exclude bubbles. Measurements were recorded in the oscillation mode at an imposed 1% strain amplitude (γ), ensuring that both moduli G' and G'' were obtained in the linear viscoelastic regime.

All measurements were carried out at 25 and 70°C. Tests were repeated at least twice to insure good repeatability of the results.

2.3.2 Electrochemical characterization

Ionic conductivity (σ_{DC}) measurements were performed via dielectric spectroscopy on a Novocontrol Broadband Dielectric Spectrometer equipped with high resolution Alpha analyzer and a Quatro temperature controller (Novocontrol GmbH). To avoid any influence of moisture/humidity on the ionic conductivity of polyelectrolytes, the latter were preliminary dried at 60 °C/1 mm Hg for 12 h in the B-585 oven (Buchi Glass Drying Oven, Switzerland) filled with P_2O_5 and then transferred under vacuum inside an argon-filled glovebox (MBRAUN MB-Labstar, H_2O and O_2 content <0.5 ppm). Polymers were sandwiched between two stainless steel (SS-316) blocking electrodes. The distance between the electrodes was kept equal to 250 μm using a Teflon spacer ring with the inner area of 0.502 cm^2. Symmetrical stainless steel/copolymer/stainless steel assembly was clamped into the 2032-coin cell and afterwards was taken out from glovebox. The experiments were carried out at 25ºC in the 10^{-1}-10^7 Hz frequency range. To obtain the DC conductivity the real part of the conductivity σ' was plotted against the frequency and σ_{DC} was extracted from the dc-plateau of the log σ' against log frequency plots.

Cyclic voltammetry (CV) was used to determine the electrochemical stability window (ESW) of solid polymer electrolytes at 70°C. VMP3 multipotentiostat (20 V, ±400 mA, Bio-Logic Science Instruments) and ECC-Std test cells (EL-Cell GmbH) were used to carry out the electrochemical characterization. Moisture contaminations were avoided by assembling the cells inside the Ar-filled glove-box (MBraun UNILab, H_2O and O_2 content <0.5 ppm). The two-electrode cells were assembled by sandwiching copolymers between the working electrode and the lithium metal foil, which served as both the reference and the counter electrodes. Carbon-coated aluminum and copper disks were used as working electrodes during anodic and cathodic stability measurements, respectively. To evaluate the oxidation limit, potential sweeps were carried out between OCV and 5 V vs. Li^+/Li at a constant rate of 0.1 mV s^{-1} at 70ºC. To determine cathodic limits, potential sweeps were performed between OCV and -0.5 V vs. Li^+/Li at the same constant rate.

The lithium-ion transference number (t_{Li^+}) was determined at 70°C in a symmetric Li metal/poly[(LiM$_{17}$-*r*-PEGM$_{86}$)-*b*-PhEtM$_{131}$]/Li metal cell, which was subjected to a 100 mV polarization bias (ΔV) with the aim to determine the initial (I_o) and the steady state (I_{ss}) currents. Electrochemical impedance spectroscopy (EIS) was performed on VMP3 multipotentiostat (20 V, ±400 mA, Bio-Logic Science Instruments) by applying a 50 mV perturbation between 500 kHz and 1 Hz at OCV conditions to obtain the resistance of the passivation layer before ($R_{SEI+CT,o}$) and after ($R_{SEI+CT,ss}$) polarization. The t_{Li^+} was calculated using the Abrahams [3] equation (4), which is the slightly modified version of the known equation proposed by Evans/Vincent/Bruce [4]:

$$t_{Li+} = \frac{I_{ss} \cdot R_{b,ss} \cdot (\Delta V - I_o \cdot R_{SEI+CT,o})}{I_o \cdot R_{b,o} \cdot (\Delta V - I_{ss} \cdot R_{SEI+CT,ss})} \quad (4),$$

where t_{Li+} is the Li transference number, ΔV is the potential applied across the cell, $R_{SEI+CT,o}$ and $R_{SEI+CT,ss}$ are the initial and the steady-state resistances of the passivating layer, I_o and I_{ss} are the initial and steady-state currents, $R_{b,o}$ and $R_{b,ss}$ are the variation of bulk electrolyte resistance.

2.3.3 Li cells assembly and testing

A composition of 60 wt.% of carbon coated $LiFePO_4$, 10 wt.% of C_{65} carbon black and 30 wt.% of poly[(LiM$_{17}$-*r*-PEGM$_{86}$)-*b*-PhEtM$_{131}$] was used for the preparation of the composite cathode in the form of catholyte. Firstly, LFP active material powder and C_{65} carbon black were gently mixed in a hand mortar and, successively added to the ca. 5-7 wt.% solution of block copolymer in anhydrous NMP upon stirring. The stirring was continued at ambient temperature for 1 h, whereupon the resultant suspension was additionally homogenized using an Ultra-Turrax® mixer (IKA-Werke GmbH & Co. KG) for 10 min. The obtained dense slurry was cast onto an aluminum current collector using a doctor-blade with a blade height of 250 μm. NMP solvent was removed by evaporation at ambient temperature for 12 h and cathode tape was further dried at 60°C/1 mm Hg for 24 h in the B-585 oven (Buchi Glass Drying Oven) filled with P_2O_5. Without connection to atmosphere the cathode tape was further transferred under vacuum inside an argon-filled glovebox (MBRAUN MB-Labstar, H_2O and O_2 content <0.5 ppm). The obtained composite cathode film had an average thickness of 85±2 μm and an active mass loading of 3.9 mg cm^{-2}.

Lab-scale Li/poly[(LiM_{17}-*r*-$PEGM_{86}$)-*b*-$PhEtM_{131}$]/$LiFePO_4$ cell prototype assembly was performed inside the Ar-filled glovebox using the ECC-Std test cells (EL-Cell GmbH). Polyethylene terephthalate (Mylar®) round spacer with a 10 mm internal diameter and a thickness of 100 μm was layered on top of the composite cathode tape. Afterwards, a layer of poly[(LiM_{17}-*r*-$PEGM_{86}$)-*b*-$PhEtM_{131}$] electrolyte was applied manually directly onto the surface of the composite LFP-based cathode within the internal diameter of the spacer. The assembly was completed with a lithium metal disk anode in a classical sandwiched configuration. The cells were galvanostatically cycled on a LBT multipotentiostat (±5V, ±5A Arbin Instruments) at 70°C between 2.5 and 4 V vs. Li^+/Li. The long-term stability test was performed at fixed charge/discharge current regime of C/20, corresponding to a full discharge or full charge of the theoretical LFP capacity (170 mAh g^{-1}) in 20 hours. Rate capability test at increasingly higher current rates was performed, where the rate is denoted as C/n, corresponding here to a full discharge or full charge of the theoretical cathode capacity (C) in n hours.

3. Results and discussion

3.1. Random poly[LiM_n-r-$PEGM_m$] copolymers

3.1.1. Synthesis

In the present work, the random RAFT copolymerization of LiM and PEGM was used for the synthesis of an ionic block (AB) (Scheme 2). The decision to combine these monomers in a statistical way was performed taking into account several facts. To increase Li^+ conduction in SICP, the -CH_2CH_2O- (EO) groups should preferably be incorporated into the short side chains; this improves local chain mobility and the effectiveness of Li ions solvation, thus allowing them to move with liquid-like mobility from side chain to side chain [13,38,40,41]. Indeed, in PEO-based SICP block copolymers, where EO-groups were located in the main polymer chain, the crystallization took place, which was significantly decreasing the charge transfer efficiency at ambient temperature [25,48–51]. As it was shown previously [26,28,33,36,37,52], all the copolymers synthesized from ionic monomers and PEGM were amorphous and none of them tend to crystalize. Moreover, the incorporation of PEGM monomer into such copolymers led to a significant decrease in their T_g, which also positively affected their ionic conductivity. Finally, as the reactivity of both monomers was found to be equal [33],

the synthesis of random copolymers represents a much simpler approach in comparison with block copolymer preparation or with the chemical bonding of already prepared polyethyleneoxide (PEO) to an ionic polymer.

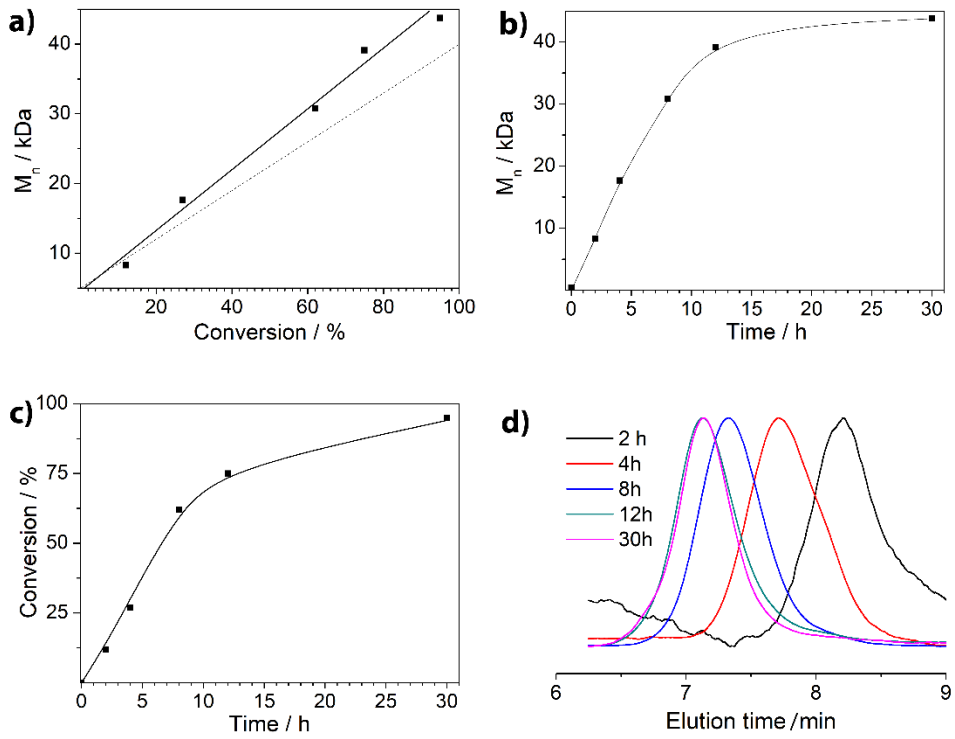

Fig.1. $M_{n\ (SEC)}$ vs. conversion (***a***), $M_{n\ (SEC)}$ vs. time (***b***) and conversion vs. time (***c***) kinetic plots for LiM and PEGM RAFT copolymerization; SEC traces of poly[LiM_n-***r***-$PEGM_m$] (***d***); Reaction conditions: DMF, CPAD:AIBN = 5:1 by mol, LiM:PEGM = 1:7 by mol, [LiM+PEGM] = 0.32 g ml^{-1} or 25 wt%, $M_{n\ theor}$ = 40.0 kDa.

RAFT copolymerization of LiM and PEGM was carried out in DMF at 60°C with 4-cyano-4-(phenylcarbonothioylthio)pentanoic acid (CPAD) as the chain transfer agent and 2,2'-azobisisobutyronitrile (AIBN) as the initiator (Scheme 2). The study of LiM-PEGM RAFT copolymerization kinetics was initially performed by an example of CPAD:[LiM+PEGM] ratio, set to target a theoretical molecular weight ($M_{n\ theo}$) of 40 kDa (Fig. 1). The probes were taken from the reaction at different times and each sample was analyzed by ^1H NMR and SEC to evaluate monomer conversion and polymer molecular weight, respectively. It was revealed that LiM and PEGM copolymerize at 60°C in a controlled manner: a linear increase in number average molecular weight ($M_{n(SEC)}$) with

the rise in conversion was observed in parallel with the achievement of satisfactory low dispersity indexes $M_w/M_n < 1.27$ (Fig. 1a). The SEC traces of the poly[LiM_n-*r*-$PEGM_m$] samples obtained at different reaction times (Fig. 1d) present unimodal peaks with decreasing elution times and reducing width, thus proving the control over polymerization. The almost full conversion (95%) was reached after 30 h (Fig. 1c). The experimental $M_{n\,(SEC)}$ values determined by SEC in 0.1 M solution of LiTFSI in DMF at 50°C were nearly equal to those obtained by NMR ($M_{n(NMR)}$), in accordance with equation (1) and only slightly higher than the theoretically calculated ones.

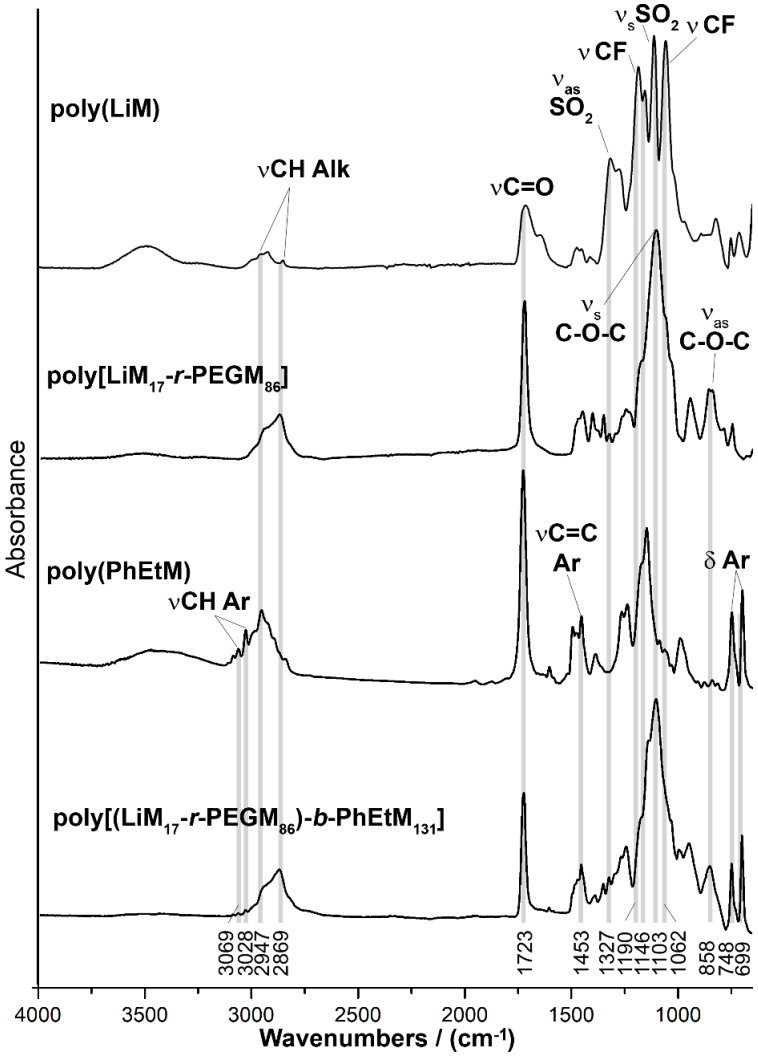

Fig. 2. IR spectra of poly(LiM), poly[LiM_{17}-*r*-$PEGM_{86}$], poly(PhEtM) and poly[(LiM_{17}-*r*-$PEGM_{86}$)-*b*-$PhEtM_{131}$].

The chemical structure, composition and purity of poly[LiM_n-*r*-$PEGM_m$] copolymers were comprehensively supported by elemental analysis, ^{1}H, ^{19}F, ^{7}Li NMR- and FTIR-spectroscopy (Fig. 2 and experimental section). FTIR spectra of copolymers showed the absorption bands at 2947 and 2872 cm^{-1} assigned to aliphatic CH_2 stretching (Fig. 2). The characteristic absorption bands of -SO_2-N-SO_2CF_3 anions were observed at 1352 (asymmetric S=O), 1179 (CF), 1055 (CF) cm^{-1}, respectively. A sharp intense peak appearing at 1723 cm^{-1} was ascribed to the ester carbonyl group (C=O) stretching vibration. The absorption bands at 1105 and 858 cm^{-1} were attributed to the asymmetric and symmetric C−O−C vibrations of the ether groups. Finally, the absence of any residual monomers was proven by the disappearance of the band at 1638 cm^{-1} (C=C).

Once the optimal reaction conditions were established, a set of poly[LiM_n-*r*-$PEGM_m$] copolymers with molecular weights in the range of 31.9 - 55.0 kDa and different in terms of LiM:PEGM ratio (from 1:3 to 1:10) were obtained via RAFT copolymerization (Table S2). To gain better control over polymerization, the duration of RAFT copolymerization was reduced to 15 h, thus limiting the total conversion of LiM and PEGM to 85.7 ÷ 87.6%. In all cases, the copolymer dispersity values were satisfactorily low ≤ 1.32, while the measured molecular weights ($M_{n(SEC)}$ and $M_{n(NMR)}$) were close to the theoretical ones (Tables S2).

3.1.2. Properties

The solubility of the obtained poly[LiM_n-*r*-$PEGM_m$] copolymers was studied in a variety of solvents. It was found that they were readily soluble in water, alcohols, acetone, acetonitrile, THF and aprotic polar solvents (DMF, DMSO, DMAc and NMP).

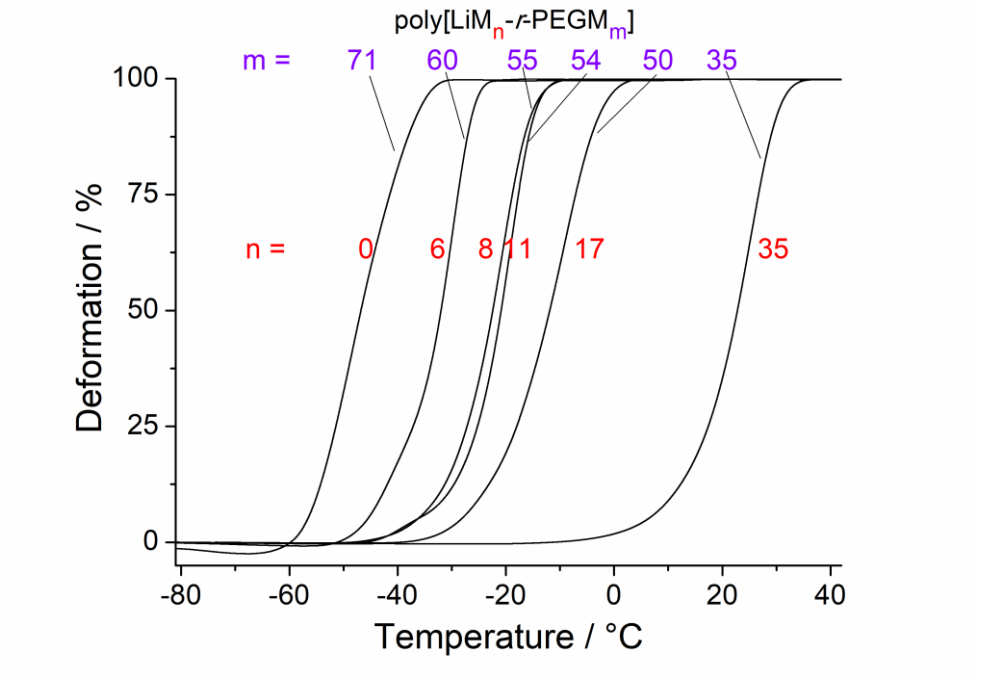

Fig. 3. TMA traces poly(PEGM) and of random poly[LiM$_n$-***r***-PEGM$_m$] copolymers.

Thermal properties of random copolymers were investigated by thermal mechanical analysis (TMA). Figure 3 shows the TMA curves of poly[LiM$_n$-*r*-PEGM$_m$] having different LiM:PEGM ratios and a fixed $M_{n\,(NMR)}$ = 30.0 ÷ 32.4 kDa.

According to TMA (Figure 3), random samples demonstrated low T_g varying in the range of -47 ÷ +15 °C, which, depending on the LiM content, can be arranged in the following decreasing order (Table S2):

T_g = 15°C poly[LiM$_{35}$-*r*-PEGM$_{35}$] > -21 poly[LiM$_{17}$-*r*-PEGM$_{50}$] > -29 poly[LiM$_{11}$-*r*-PEGM$_{54}$] > -31 poly[LiM$_8$-*r*-PEGM$_{55}$] > -47 poly[LiM$_6$-*r*-PEGM$_{60}$] > -57 poly(PEGM)$_{71}$

Overall, the higher was the LiM content, the higher was the T_g observed in copolymers having the same molar mass. The increase in the molecular weight of copolymers from $M_{n\,(NMR)}$ = 30.8 to 49.1 kDa having the same ratio of LiM:PEGM (1:5) led only to a slight rise in T_g from -29 to -25°C (Table S2, entries 3-4). It should be noted that all poly[LiM$_n$-*r*-PEGM$_m$] samples demonstrated only one glass transition in the TMA curves, being exactly in between the transitions attributed to neat poly(PEGM) (T_g= -57°C, Fig. 3, n=0, m=71) and poly(LiM) (T_g=105°C [52]), thus proving the formation of random copolymers. The results reported here are in full agreement with those published

previously for random copolymers based on LiSTFSI and poly(ethylene glycol)methyl ether acrylate monomers [26].

Ionic conductivity measured for random poly[LiM$_n$-*r*-PEGM$_m$] copolymers revealed an interesting behavior, showing a maximum at 4.6×10^{-7} S/cm (25°C) in between the ionic conductivities for poly[LiM$_{17}$-*r*-PEGM$_{50}$] and poly[LiM$_{11}$-*r*-PEGM$_{54}$] (Fig. 4). Starting from poly[LiM$_6$-*r*-PEGM$_{60}$], the ionic conductivity increased with the growth in Li^+ number up to poly[LiM$_{11}$-*r*-PEGM$_{54}$]. However, the subsequent growth of LiM content led to the decrease in conductivity down to 1.3×10^{-8} S/cm (25°C) for poly[LiM$_{35}$-*r*-PEGM$_{35}$]. It can be explained by the fact that at PEGM/LiM = 5÷10 mole ratio, the polyelectrolyte conductivity improved with the increase in concentration of charge carriers (Li^+). The ion/EO chains coordination and the ions hopping transport occurred due to the high mobility of the copolymer side chain segments. After a certain PEGM/Li ratio (< 3), the T_g of the copolymers started to increase, thus reducing the chains mobility and, in its turn, decreasing the ionic conductivity.

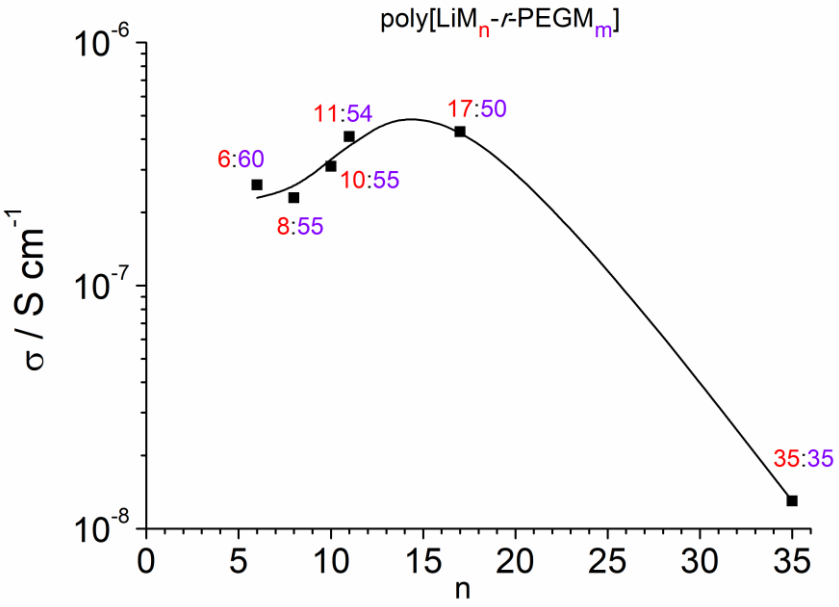

Fig. 4. Ionic conductivity at 25°C vs. number of LiM monomer units (n) in poly[LiM$_n$-***r***-PEGM$_m$] at a fixed M$_{n\ (NMR)}$~30 kDa.

3.2. Block poly[(LiM$_n$-r-PEGM$_m$)-b-PhEtM$_k$] copolymers

3.2.1. Synthesis

The synthesized random poly[LiM$_n$-*r*-PEGM$_m$] copolymers were further applied as macro-chain-transfer agents (macro-CTAs) in the synthesis of poly[(LiM$_n$-*r*-PEGM$_m$)-*b*-PhEtM$_k$] block copolymers (Table 1 and S3). For more accurate calculations in the synthesis of block copolymers and comparison of their molecular weights, the $M_{n(NMR)}$ values determined by eq. 1-3 (see experimental section) were further used.

The 2-phenylethyl methacrylate (PhEtM) was chosen for the preparation of the B-block for several reasons (Scheme 2). First, this monomer contains methacrylic functional group similar to LiM and PEGM that will insure the successful realization of the block copolymers synthesis with the same CPAD RAFT agent. Second, PhEtM possesses the aromatic moiety which is incompatible with polar LiM and PEGM based polymers. In addition, poly(PhEtM) shows the T_g equal to 39^{o}C (Fig. S4), thus providing an average difference of 60-65^{o}C between the glass transition temperatures of both blocks. The work started with the investigation of PhEtM RAFT polymerization. The study of the process kinetics was carried out in DMF at 60°C with a ratio [CPAD]$_o$:[AIBN]$_o$=5:1 (Scheme 3).

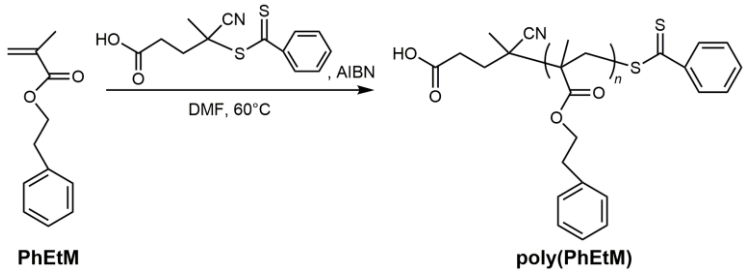

Scheme 3. RAFT polymerization of PhEtM.

The kinetic plots shown in Figure S1 demonstrated good control over the polymerization reaction: 96% monomer conversion was reached after 34 h (Fig. S1a). The M$_n$ vs. conversion plot demonstrated linear increase (Fig. S1b), while the M_w/M_n ratio remained close to 1.25 (Fig. S1c). At this, the experimental M_n values determined for poly(PhEtM) by SEC in 0.1 M solution of LiTFSI in DMF at 50°C were nearly three times lower compared to the theoretically calculated ones (Fig. S1b). This discrepancy can be explained by the structural difference between the comb-like poly(PhEtM) with aromatic substituents and poly(methyl methacrylate) (PMMA) calibration standards. Nevertheless, SEC analysis showed (Fig. S1d) monomodal shape of the peaks that were continuously shifted towards short elution times with increase in PhEtM conversion

indicating the growth of poly(PhEtM) chain. The chemical structure and purity of poly(PhEtM) was confirmed by ^{1}H NMR and IR spectroscopy (Fig. S2 and S3).

After determination of the optimal conditions for PhEtM RAFT polymerization a set of poly[(LiM$_n$-*r*-PEGM$_m$)-*b*-PhEtM$_k$] block copolymers was synthesized by RAFT polymerization of PhEtM using poly[LiM$_n$-*r*-PEGM$_m$] copolymers as macro-CTA (Scheme 2). The reaction was performed in DMF at 60°C for 15 h. The initial [macro-CTA]$_o$ / [AIBN]$_o$ ratio was kept constant (5:1), while the [PhEtM]$_o$ to [macro-CTA]$_o$ ratio was varied in order to obtain poly[(LiM$_n$-*r*-PEGM$_m$)-*b*-PhEtM$_k$] copolymers with different molecular weights (Table 1 and Table S3). The ionic content in synthesized copolymers was controlled by the n:m ratio in the used macro-CTAs (poly[LiM$_n$-*r*-PEGM$_m$]), while the control over the ratio between molecular weights of the blocks (M_A/M_B) was gained by varying the PhEtM loading. The PhEtM conversion determined by ^{1}H NMR spectroscopy was in the range of 52.1 ÷ 59.3%. The obtained poly[(LiM$_n$-*r*-PEGM$_m$)-*b*-PhEtM$_k$] block copolymers with $M_{n(NMR)}$ < 40 kDa represented wax like materials, while copolymers with $M_{n(NMR)}$ > 40 kDa exhibited rubber-like properties.

Table 1. Synthesis of poly[(LiM_n-*r*-$PEGM_m$)-*b*-$PhEtM_k$] block copolymers.

N	poly[LiM_n-*r*-$PEGM_m$] (A-block)							poly[(LiM_n-*r*-$PEGM_m$)-*b*-$PhEtM_k$] (A-b-B block copolymer)				
	polymer	$M_{n\,(target)}$ (kDa)	$M_{n\,(SEC)}$ (kDa)[a]	M_w/M_n[a] (SEC)	$M_{n\,(NMR)}$ (kDa)[b]	PEGM: LiM [c]	σ_{DC}, (S/cm) 25°C	Block copolymer	$M_{n\,(SEC)}$ (kDa)[a]	M_w/M_n[a] (SEC)	$M_{n\,(NMR)}$ (kDa)[b]	M_A/M_B[b]
1	poly[LiM_6-*r*-$PEGM_{27}$]	17.0	20.8	1.10	15.8	4.4	7.9×10^{-7}	poly[(LiM_6-*r*-$PEGM_{27}$)-*b*-$PhEtM_{53}$]	24.3	1.12	25.8	1.6:1
2	poly[LiM_{17}-*r*-$PEGM_{50}$]	35.1	38.3	1.15	30.7	3.0	4.3×10^{-7}	poly[(LiM_{17}-*r*-$PEGM_{50}$)-*b*-$PhEtM_{82}$]	43.2	1.19	46.3	2.0:1
3	poly[LiM_{11}-*r*-$PEGM_{54}$]	35.1	35.5	1.13	30.8	5.0	4.1×10^{-7}	poly[(LiM_{11}-*r*-$PEGM_{54}$)-*b*-$PhEtM_{40}$]	39.2	1.15	38.5	4.0:1
4								poly[(LiM_{11}-*r*-$PEGM_{54}$)-*b*-$PhEtM_{74}$]	43.3	1.13	44.8	2.2:1
5	poly[LiM_8-*r*-$PEGM_{56}$]	35.1	35.0	1.14	30.6	7.0	2.3×10^{-7}	poly[(LiM_8-*r*-$PEGM_{56}$)-*b*-$PhEtM_{82}$]	42.4	1.17	46.2	2.0:1
6	poly[LiM_{17}-*r*-$PEGM_{86}$]	57.7	55.0	1.16	49.1	5.0	4.1×10^{-7}	poly[(LiM_{17}-*r*-$PEGM_{86}$)-*b*-$PhEtM_{49}$]	57.7	1.21	58.4	5.3:1
7								poly[(LiM_{17}-*r*-$PEGM_{86}$)-*b*-$PhEtM_{75}$]	61.6	1.19	63.4	3.4:1
8								poly[(LiM_{17}-*r*-$PEGM_{86}$)-*b*-$PhEtM_{131}$]	67.7	1.17	74.1	2.0:1
9								poly[(LiM_{17}-*r*-$PEGM_{86}$)-*b*-$PhEtM_{194}$]	74.7	1.19	85.9	1.3:1

[a] By GPC in 0.1 M solution of LiTFSI in DMF at 50°C with PMMA standards.
[b] Defined by equations (*1*,*2*) for random or by equation (*3*) for block copolymers.
[c] By ^{1}H NMR ($CDCl_3$).

Molecular weight values of the obtained block copolymers were determined by both SEC chromatography and ^{1}H NMR (Table 1). Figure 5 shows the SEC chromatograms of the parent poly[LiM$_{17}$-*r*-PEGM$_{86}$] with $M_{n(SEC)}$ = 55.0 kDa and the subsequent increase in the molecular weight of the growing block copolymers poly[(LiM$_{17}$-*r*-PEGM$_{86}$)-*b*-PhEtM$_k$] with k = 49, 75, 131 or 194 (Table 1, lines 6-9). A clear shift of the SEC traces toward higher molecular range with M_w/M_n remaining < 1.21, confirmed the efficient polymerization initiation and clearly demonstrated the formation of the second block. The experimental $M_{n(SEC)}$ values for poly[(LiM$_{17}$-*r*-PEGM$_{86}$)-*b*-PhEtM$_k$] block copolymers were found to be lower than $M_{n(NMR)}$ calculated from the PhEtM conversion. Apparently, this can be explained by similar large difference between the experimental $M_{n(SEC)}$ and calculated M$_{n(NMR)}$ values observed for the poly(PhEtM) homopolymer noted above.

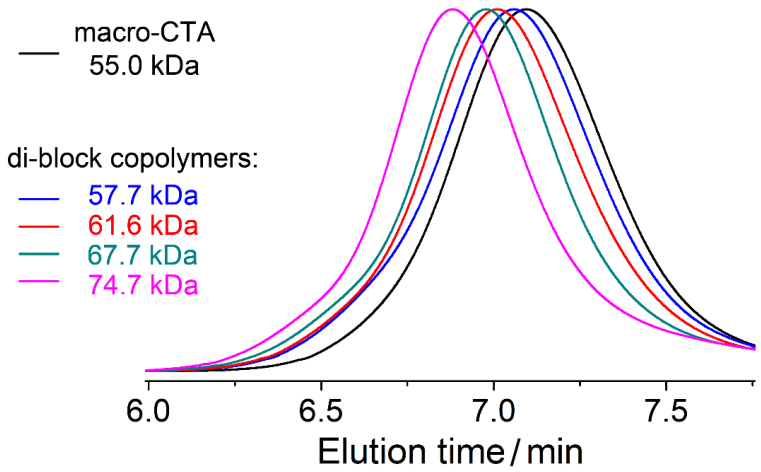

Fig. 5. SEC traces of poly[(LiM$_{17}$-*r*-PEGM$_{86}$)-*b*-PhEtM$_k$] block copolymers obtained from poly[LiM$_{17}$-*r*-PEGM$_{86}$] macro-CTA.

The chemical structure, composition and purity of poly[(LiM$_n$-*r*-PEGM$_m$)-*b*-PhEtM$_k$] block copolymers were confirmed by NMR and IR spectroscopy (Fig. 2 and 5). NMR chemical shifts corresponding to both blocks, namely to poly[LiM$_n$-*r*-PEGM$_m$] and poly(PhEtM), were clearly observed (Fig. 6). Integration of the appropriate signals depicted as *n* and *g*+*j*+*m* in Fig. 6 and attributed to Ar-C<u>H$_2$</u>-CH$_2$- from poly(PhEtM) and CO-O-C<u>H$_2$</u>- protons from all blocks, respectively, provided composition of the block copolymers and M_A/M_B ratio. The analysis of block copolymer IR spectrum (Fig. 2) confirmed the presence of both blocks. Thus, apart the characteristic absorption bands of

-SO_2-N-SO_2CF_3 anion (1350, 1175, 1137, 1028 cm^{-1}) from LiM, ether -C-O-C- groups (1103, 851 cm^{-1}) from PEGM and of ester carbonyl group C=O (1723 cm^{-1}) from all methacrylic monomer units, the signals attributed to CH-aromatic stretching (3062, 3028 cm^{-1}), CH-aromatic deformation vibrations (748, 699 cm^{-1}) and to C=C vibrations of the aromatic ring (1453 cm^{-1}) were observed as well (Fig. 2).

While poly[LiM_n-*r*-$PEGM_m$] copolymers represented very soft and sticky pink materials, the poly[(LiM_n-*r*-$PEGM_m$)-*b*-$PhEtM_k$] block copolymers appeared to be pink rubber-like elastomers that can hold the weight load (Fig. 7).

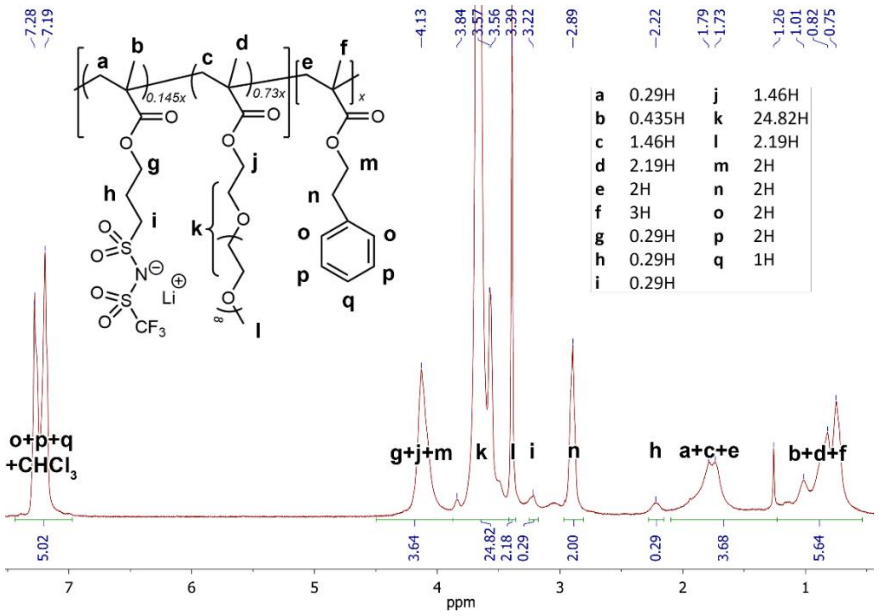

Fig. 6. ^{1}H NMR of poly[(LiM_{17}-*r*-$PEGM_{86}$)-*b*-$PhEtM_{131}$] in $CDCl_3$.

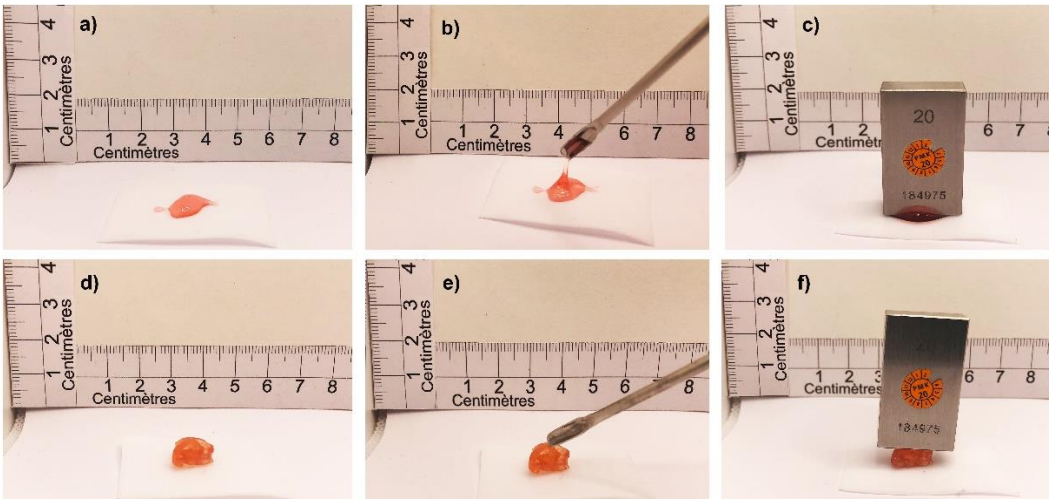

Fig. 7. Appearance and difference in mechanical robustness between poly[LiM_{17}-*r*-$PEGM_{86}$] (**a-c**) and poly[(LiM_{17}-*r*-$PEGM_{86}$)-*b*-$PhEtM_{131}$] (**d-f**) block copolymers.

3.2.2. Thermomechanical analysis

Thermal properties of poly[(LiM$_n$-*r*-PEGM$_m$)-*b*-PhEtM$_k$] block copolymers were studied by thermal mechanical analysis (TMA). Most of the samples demonstrated three transition temperatures (Table 2).

These transitions were attributed as follow: i) the first low temperature transition corresponded to the glass transition (T_{g1}) of the parent poly[LiM$_n$-*r*-PEGM$_m$] ionic block, ii) the second transition was assigned to the glass transition (T_{g2}) of the poly(PhEtM) block and iii) the final transition related to heat distortion temperature (T_{HDT}) at which a noticeable deformation was observed under applied load and scanning/heating rate. These three transition temperatures were found to be strongly dependent on the number of LiM units in the ionic poly[LiM$_n$-*r*-PEGM$_m$] block, the molecular weight of the poly(PhEtM) block, the total molar mass of the block copolymer and the ratio of ionic and nonionic blocks (M_A/M_B). These observations can be summarized as follows: i) the decrease in LiM content and increase in PEGM/LiM ratio from 3 to 7 led to the decrease in T_{g1} (Table 2, entries 1-5); ii) the increase in PhEtM units number resulted in the increase in T_{g2} (Table 2, entries 3-4 and 6-9); iii) the higher was the molecular weight of poly[(LiM$_n$-*r*-PEGM$_m$)-*b*-PhEtM$_k$] block copolymer and the lower was the M_A/M_B ratio, the higher the T_{HDT} was observed (Table 2, entries 4-5 and 7-9).

3.2.3 Ionic conductivity

Ionic conductivity (σ) of poly[(LiM$_n$-*r*-PEGM$_m$)-*b*-PhEtM$_k$] block copolymers was investigated by dielectric spectroscopy and related results are listed in the Table 2. Ionic conductivity was found to be dependent on PEGM/LiM ratio, total molecular weight of block copolymer and the ratio of ionic and nonionic blocks M_A/M_B.

When studying the effect of PEGM/LiM ratio on the ionic conductivity of block copolymers, the same trend as for parent poly[LiM$_n$-*r*-PEGM$_m$] random copolymers was detected (Table 2 and Fig. 4). Considering the series of samples, namely poly[(LiM$_{17}$-*r*-PEGM$_{50}$)-*b*-PhEtM$_{82}$], poly[(LiM$_{11}$-*r*-PEGM$_{54}$)-*b*-PhEtM$_{74}$] and poly[(LiM$_8$-*r*-PEGM$_{56}$)-*b*-PhEtM$_{82}$] (Table 2**,** entries 2, 4 and 5) with similar values of $M_{n(NMR)}$ = 44.8÷46.3 kDa and M_A/M_B=2.0÷2.2, the highest ionic conductivity (σ = 9.5×10^{-8} S/cm, 25°C) was obtained for the block copolymer with PEGM/LiM = 5, while for samples with PEGM/Li = 3 and 7, σ was lower (3.0×10^{-8} and 5.0×10^{-8} S/cm, respectively). Another trend was

Table 2. Selected properties of poly[(LiM$_n$-*r*-PEGM$_m$)-*b*-PhEtM$_k$] block copolymers.

N	poly[(LiM$_n$-*r*-PEGM$_m$)-*b*-PhEtM$_k$]	M_A/M_B[a]	T_{g1}, (°C)[b]	T_{g2}, (°C)[b]	T_{HDT}, (°C)[b]	σ_{DC}, (S/cm) at 25°C	Type of morfology[c]	Domain length (nm)	Cylinders diameter (nm)
1	poly[(LiM$_6$-*r*-PEGM$_{27}$)-*b*-PhEtM$_{53}$]	1.6:1	-39	35	67	2.6×10^{-8}	disordered	-	-
2	poly[(LiM$_{17}$-*r*-PEGM$_{50}$)-*b*-PhEtM$_{82}$]	2.0:1	-47	34	93	3.0×10^{-8}	HPC[d]	25.4±0.9	16.6±4.4
3	poly[(LiM$_{11}$-*r*-PEGM$_{54}$)-*b*-PhEtM$_{40}$]	4.0:1	-48	23	-	7.8×10^{-8}	HPC	16.3±0.1	10.6±3.6
4	poly[(LiM$_{11}$-*r*-PEGM$_{54}$)-*b*-PhEtM$_{74}$]	2.2:1	-51	26	69	9.5×10^{-8}	HPC	22.8±1.8	13.7±3.1
5	poly[(LiM$_8$-*r*-PEGM$_{56}$)-*b*-PhEtM$_{82}$]	2.0:1	-51	21	75	5.0×10^{-8}	HPC	18.6±3.4	11.9±2.4
6	poly[(LiM$_{17}$-*r*-PEGM$_{86}$)-*b*-PhEtM$_{49}$]	5.3:1	-48	25	-	2.8×10^{-7}	HPC	18.9±1.6	12.8±2.7
7	poly[(LiM$_{17}$-*r*-PEGM$_{86}$)-*b*-PhEtM$_{75}$]	3.4:1	-49	31	76	2.3×10^{-7}	HPC	29.7±1.4	18±4.1
8	poly[(LiM$_{17}$-*r*-PEGM$_{86}$)-*b*-PhEtM$_{131}$]	2.0:1	-48	33	92	3.8×10^{-7}	lamellar	34.1±1.2	-
9	poly[(LiM$_{17}$-*r*-PEGM$_{86}$)-*b*-PhEtM$_{194}$]	1.3:1	-49	51	120	3.4×10^{-7}	lamellar	38.7±0.8	-

[a] Defined by equation (*3*).
[b] By TMA.
[c] By AFM on block copolymer coatings.
[d] Hexagonally packed cylinders.

observed for block copolymers having closed PEGM/LiM (4.4÷5.0) and M_A/M_B (1.6÷2.2) ratios, but different molecular weights, $M_{n(NMR)}$ = 25.8, 44.8 and 74.1 kDa (Table 2, lines 1, 4, 8). Actually, an almost 3 times increase in the $M_{n(NMR)}$ was accompanied by nearly 14 times increase in ionic conductivity (from 2.6×10^{-8} to 3.8×10^{-7} S/cm at 25°C). Thus, in terms of charge transfer efficiency, the poly[(LiM$_{17}$-*r*-PEGM$_{86}$)-*b*-PhEtM$_{131}$] block copolymer was almost equal to the parent poly[LiM$_{17}$-*r*-PEGM$_{86}$], despite the decrease in the concentration of Li cations (3.8×10^{-7} and 4.1×10^{-7} S/cm at 25°C, respectively).

The molecular weight of poly(PhEtM) block and the M_A/M_B ratio were found to influence the ionic conductivity of block copolymers as well (Table 2, lines 3-4 and 6-9). In poly[LiM$_{11}$-*r*-PEGM$_{54}$] based block copolymers the increase in PhEtM units content led to the rise in ionic conductivity from 7.8×10^{-8} to 9.5×10^{-8} S/cm at 25°C (Table 2, entries 3-4). In the series of poly[(LiM$_{17}$-*r*-PEGM$_{86}$)-*b*-PhEtM$_k$] block copolymers, the increase in ionic conductivity with the increase of PhEtM units from 49 to 194 was less pronounced (Table 2, entries 6-9 and Fig. 8). However, it still doubled from 2×10^{-7} to 4×10^{-7} S/cm at 25°C.

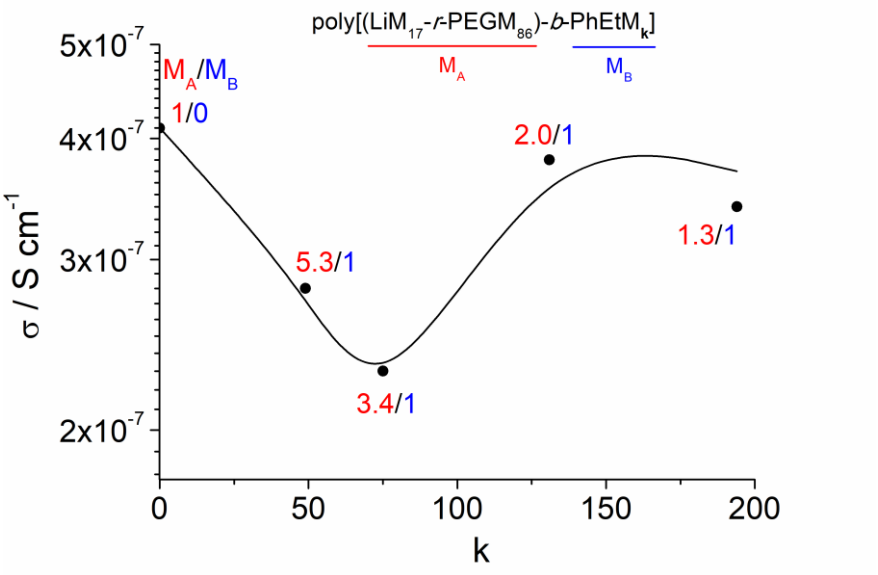

Fig. 8. Ionic conductivity at 25°C vs. number of PhEtM units (**k**) in poly[(LiM$_{17}$-*r*-PEGM$_{86}$)-*b*-PhEtM$_k$] block copolymers.

The last two trends are in contradiction with the concentration of the mobile charges in the copolymer. Commonly, the increase in non-coordinating monomer content should

result in the overall decrease in ionic conductivity because of reduction of conducting species. However, as it was proposed at the beginning of the work, the synthesis of the block copolymers with two immiscible blocks supposed to lead to the microphase segregation, which in turn can explain the conductivity results (see vide infra).

The temperature dependence of ionic conductivity for the best poly[(LiM$_{17}$-*r*-PEGM$_{86}$)-*b*-PhEtM$_{131}$] block copolymer is shown in Figure 9. Electrochemical impedance spectroscopy (EIS) analysis was carried out between 25 and 120 °C. The Arrhenius plot shows ionic conductivity increase with the rise in temperature, reaching practical values in the order of 10^{-6} and 10^{-5} S/cm at 40 and 80 °C, respectively. The plot slightly deviates from the ideal linear Arrhenius behavior especially at temperature below 40 °C (T_{g2} of copolymer), indicating inter-relation between the conductivity and segmental relaxation of polymer segments. On the contrary, at elevated temperatures, the deviation from the linear dependence is less pronounced, suggesting that, in the range of 50-90 °C, the Li^+ ion diffusion occurs prevalently through hopping on anionic sites. The curve gradient modification above 90 °C is likely associated with the third phase transition (T_{HDT}) and the formation of a disordered system.

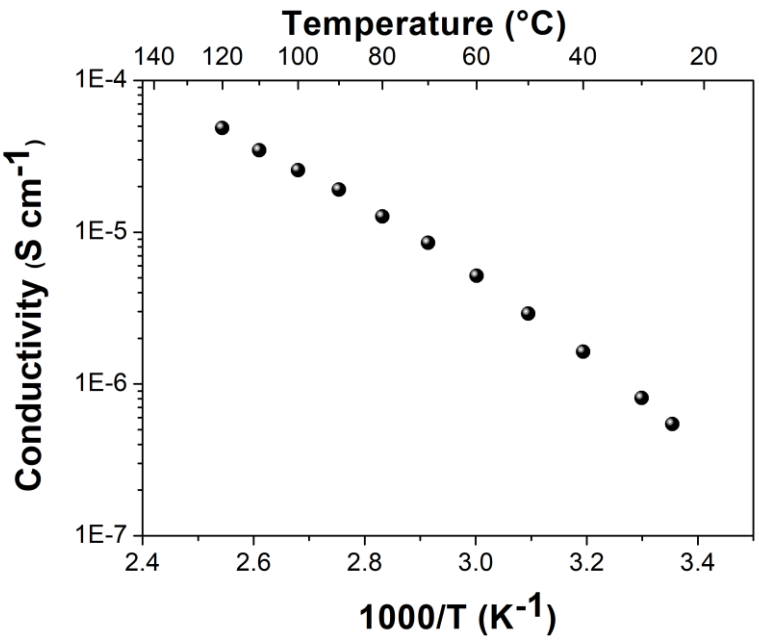

Fig. 9. Ionic conductivity vs. temperature dependence for poly[(LiM$_{17}$-*r*-PEGM$_{86}$)-*b*-PhEtM$_{131}$].

3.2.4. Morphological phase behavior

The presence of the two distinct glass transitions temperatures on TMA curves of all poly[(LiM$_n$-*r*-PEGM$_m$)-*b*-PhEtM$_k$] block copolymers clearly demonstrated the presence of two segregated microphases. To prove this conclusion and to determine the type of morphology, thin coatings of block copolymers were studied by AFM (Fig. 10 and Table 2). AFM images of phase shift revealed that the bulk block copolymers mesoscopic self-assembly fits into two categories: perpendicular hexagonally packed cylinders (HPC) and perpendicular lamellas (Fig. 10 and Fig. S5). The only exception was found for sample poly[(LiM$_6$-*r*-PEGM$_{27}$)-*b*-PhEtM$_{53}$] that did not exhibit any visible phase separation on AFM images (Table 2, entry 1). This result can be explained by the low molecular weight of copolymer blocks, resulting in a low incompatibility of polymer blocks allowing disorder in chains arrangement (Figs. S5a-S5b). With the increase in molecular weight of blocks, the incompatibility of the chains increased, and a mesoscopic phase separation occurred under HPC perpendicular to the bulk surface (Table 2, entries 2-7, Fig. 10a-10d, Fig. S5c-S5h). The subsequent increase in both number of PhEtM units and total molecular weight of block copolymers ended up in a new arrangement of chains to reduce stretching, thus leading to a lamellar type nanophase separation perpendicular to the surface [53] (Table 2, entries 8-9, Fig. 10e-10j).

The domain size was found to be dependent on several factors are summarized in the followings:

1. PEGM/LiM ratio. In block copolymers with molecular weight $M_{n(NMR)}$ = 44.8 ÷ 46.3 kDa and M_A/M_B ratio = 2: 1, the diameter of the cylinders and the distance between them were found to be dependent on the composition of the ionic block (Table 2, entries 2, 4-5). As the number of PEGM units was increased (PEGM/LiM ratio increased from 3 to 7), the distance between the cylinders and their diameter showed a gradual decrease (from 25.4 to 18.6 nm and from 16.6 to 11.9 nm, respectively).

2. M_A/M_B ratio and poly(PhEtM) content (k). The influence of such a parameter as M_A/M_B ratio on the size and type of the domains can be traced by the example of low and high molecular weight block copolymers having fixed PEGM/LiM ratio equal to 5 (Table 2, entries 3-4 and 6-9). In both series, with the increase in poly(PhEtM) content (k) the size of the domains was increasing from 16.3 to 25.4 nm and from 18.9 to 38.7 nm, respectively.

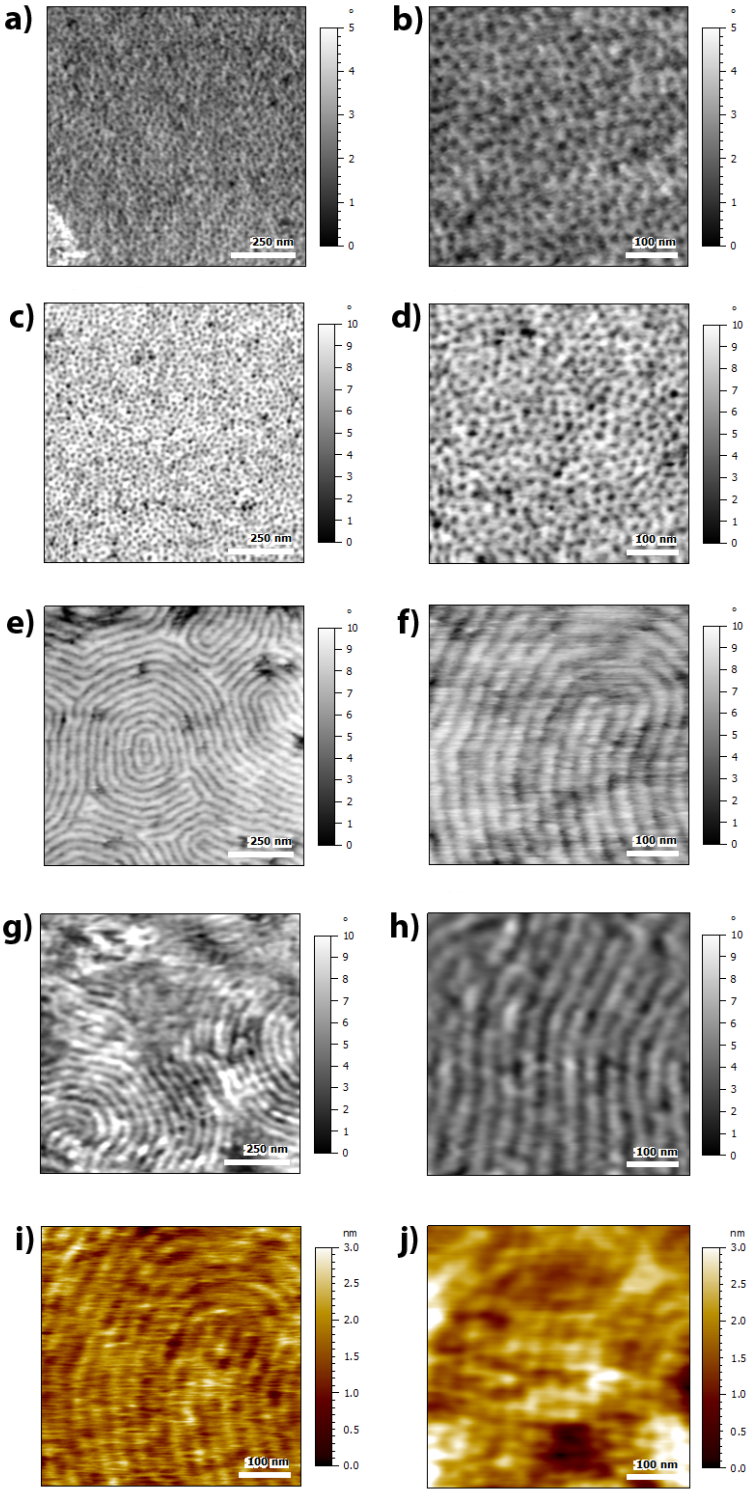

Fig. 10. AFM images of poly[(LiM$_{11}$-*r*-PEGM$_{54}$)-*b*-PhEtM$_{74}$] (a, b), poly[(LiM$_{8}$-*r*-PEGM$_{56}$)-*b*-PhEtM$_{82}$] (c, d), poly[(LiM$_{17}$-*r*-PEGM$_{86}$)-*b*-PhEtM$_{131}$] (e, f) and poly[(LiM$_{17}$-*r*-PEGM$_{86}$)-*b*-PhEtM$_{194}$] (g, h) films at different resolutions. Topography of poly[(LiM$_{17}$-*r*-PEGM$_{86}$)-*b*-PhEtM$_{131}$] (i) and poly[(LiM$_{17}$-*r*-PEGM$_{86}$)-*b*-PhEtM$_{194}$] (j) coatings.

Upon reaching a certain value of $M_A/M_B \leq 2.0$ for high molecular weight block copolymers, the type of microphase was changing: the hexagonally packed cylinders were transforming into the lamellar morphology (Table 2, entries 6-9 and Fig. 10e-10j). The same trend was observed for diameters of the cylinders that were increased in size from 10.6 to 13.7 and from 12.8 to 18.0 nm when k was raised from 40 to 74 and from 75 to 131 (Table 2, entries 3-4 and 7-8), thus suggesting that the centers of the cylinders were occupied by poly(PhEtM) chains.

3. Overall molecular weight of block copolymer. With the growth in the molecular weight of the block copolymers with constant PEGM/LiM and M_A/M_B ratios (5:1 and ~2.0, correspondingly) the probability of microphase separation increased (Table 2, entries 1, 4, 8). The sample with low molecular weight ($M_{n(NMR)}$ = 25.8 kDa) showed only disordered structure (Table 2, entry 1). The increase in $M_{n(NMR)}$ up to 44.8 kDa led to the formation of hexagonally packed cylinders, while further growth of $M_{n(NMR)}$ to 74.1 kDa was accompanied by a transition to lamellar morphology.

As above mentioned, the ionic conductivity in poly[(LiM_{17}-*r*-$PEGM_{86}$)-*b*-$PhEtM_k$] block copolymers unexpectedly increased with the increase in molecular weight. After morphological investigation, it is possible to conclude that the increase in ionic conductivity benefits from the formation of the long-range-ordered lamellas in comparison with cylindrical phase separation (Table 2, entries 6-9). It can be further speculated that samples exhibiting hexagonally packed cylindrical morphology have a low degree of long-range order and the decrease in in-plane ionic conductivity likely results by numerous morphological defects and large numbers of grain boundaries that serve as "dead ends" for conductive channels [54]. In contrast, when the microphase segregation yields the lamellar structures, the continuous ion-conducting pathways with high concentration of Li^+ cations and ethylene oxide solvating groups are formed, that in its turn facilitates the ion transport and increases the overall ionic conductivity. These results perfectly correlate with those observed for cationic block copolymers reported previously [43,47,54].

3.2.5. Rheological (mechanical) properties

As the investigation of the viscoelastic properties is an indirect method for the estimation of mechanical performance of elastomeric materials, the dynamic rheological

properties of poly[(LiM$_{17}$-*r*-PEGM$_{86}$)-*b*-PhEtM$_{131}$] block copolymer with the highest ionic conductivity and lamellar microphase segregation were measured by carrying out rheological measurements in a small amplitude oscillatory flow mode at 25 and 70°C (Fig. 11).

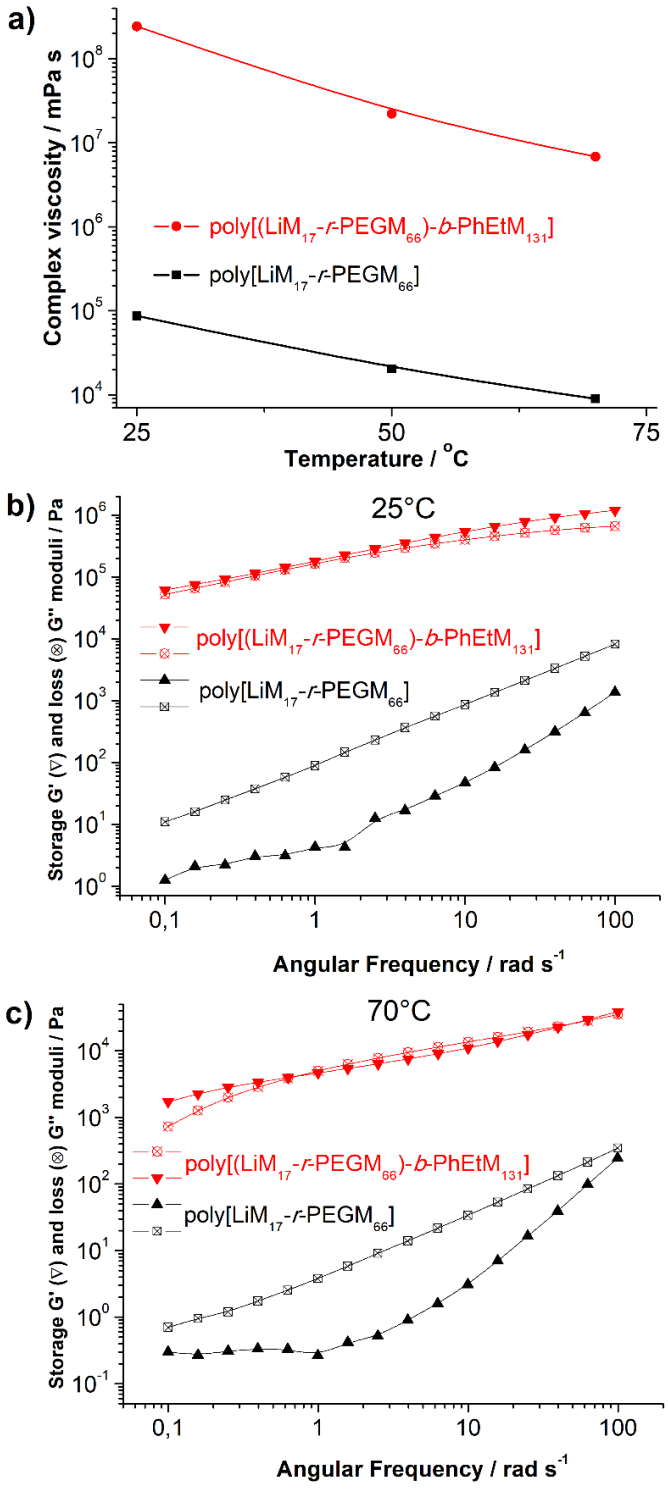

Fig. 11. Temperature dependence of the complex viscosity (a) and frequency dependence of the storage modulus G' (full symbols) and the loss modulus G" (open symbols) obtained at 25 (b) and 70 °C (c) for poly[(LiM$_{17}$-*r*-PEGM$_{86}$)-*b*-PhEtM$_{131}$] and poly[LiM$_{17}$-*r*-PEGM$_{86}$].

They were further compared to those demonstrated by parent poly[LiM$_{17}$-*r*-PEGM$_{86}$] random copolymer. Fig. 11a shows the temperature dependence of complex viscosity at a constant frequency of 1 Hz. The curves of both copolymers demonstrated smooth decrease with the increase of temperature having nearly the same slope. At any temperature poly[(LiM$_{17}$-*r*-PEGM$_{86}$)-*b*-PhEtM$_{131}$] possessed significantly higher complex viscosity than the parent poly[LiM$_{17}$-*r*-PEGM$_{86}$] (Fig. 11a). The observed enhancement in viscoelastic behavior reached up to four orders of magnitude.

Figures 11b and 11c show the storage and loss moduli versus angular frequency dependence performed at 25 and 70°C. For poly[LiM$_{17}$-*r*-PEGM$_{86}$], the imaginary part (*G*") exceeded the real part (*G*') of the complex modulus over the entire frequency range and at all temperatures. Both moduli exhibited high degree of frequency dependence. Such behavior of poly[LiM$_{17}$-*r*-PEGM$_{86}$] can be ascribed as the one closed to a liquid-like or molten state. In contrast, for poly[(LiM$_{17}$-*r*-PEGM$_{86}$)-*b*-PhEtM$_{131}$] the *G*' was higher than *G*" or nearly coincided with it at both temperatures. Moreover, both *G*' and *G*" were less frequency dependent for the block copolymer than for the parent random copolymer over the entire measured range. This behavior of poly[(LiM$_{17}$-*r*-PEGM$_{86}$)-*b*-PhEtM$_{131}$] can be attributed to the one having solid-like character. Finally, block copolymer demonstrated the improvement in both moduli up to five orders of magnitude.

The observed improvement in viscoelastic behavior can only be explained by the presence of stiff PhEtM block as both compared copolymers are linear and have the ionic poly[LiM$_{17}$-*r*-PEGM$_{86}$] block of the same molecular weight. These results are of high importance as solid polymer electrolytes with increased stiffness were previously reported to effectively suppress/limit the growth of lithium dendrites [55,56].

3.2.6. Li^+ ion transference number and electrochemical stability

The promising prospects of the newly developed single-ion conducting polymer electrolyte were further confirmed by testing poly[(LiM$_{17}$-*r*-PEGM$_{86}$)-*b*-PhEtM$_{131}$] block

copolymer in terms of lithium ion transference number (t_{Li}^{+}) and anodic stability window (ASW). The t_{Li+} was determined by the method of Abraham et al. [57,58] as detailed in experimental. The typical Nyquist plots of a.c. impedance of a Li/poly[(LiM$_{17}$-*r*-PEGM$_{86}$)-*b*-PhEtM$_{131}$]/Li symmetrical cell at 70°C are shown in Fig. S6. The cell Nyquist plot did not change significantly during the experiment, and the initial bulk resistance (R_b) value of 2958 Ω only decreased to 2928 Ω, while the charge transfer resistance (R_{ct}) showed only a limited drop from 250 Ω to 238 Ω, thus proving a stable interfacial contact with the lithium metal electrode. The plot of the current response to the applied bias as a function of time is shown in Fig. S7. A current drop from 23.46 μA to 22.74 μA was observed before the steady state was reached. It resulted in a calculated t_{Li}^{+} value of 0.96; a high value, which is fundamental to reduce concentration polarization of electrolytes during charge–discharge steps, thus producing higher power density. It is fully in agreement with Li transference number values published for similar SICPs previously [13,14,38]. Clearly, such value is noticeably higher than values reported for "standard" liquid electrolytes containing dissolved Li salts, including IL-based electrolytes, cationic PILs/Li salts and/or salt in polymers (e.g., PEO/Li) [11,13,59–61].

The ESW of the single-ion poly[(LiM$_{17}$-*r*-PEGM$_{86}$)-*b*-PhEtM$_{131}$] block copolymer was investigated by cyclic voltammetry at 70 °C. The results are shown in Fig. S8. The anodic breakdown potential of the sample was found to be close to 4.4 V vs. Li^+/Li. At such potential value, the current increase was likely associated with the partial decomposition of ethylene oxide containing moieties and TFSI functional groups in the polymer electrolyte [62]. During the second cycle, the intensity of the peaks largely decreased, along with a shift of the anodic limit up to 4.5 V vs. Li^+/Li, which likely accounts for the growth of a passivation layer at the electrode/electrolyte interface. On the other hand, the first cathodic reduction presents almost undetectable current peaks likely associated to the reduction/decomposition process of residual solvent traces from the synthesis. Indeed, highly reversible couple of peaks are observed between -0.5 and 0.5 V versus Li^+/Li, which are clearly associated with lithium plating/stripping process, confirming the efficient transfer of lithium ions through the polyelectrolyte. The value of ESW, obtained for the newly synthetized block copolymer accounts for stable and safe operation with cathodes operating at medium-high voltage, such as commercially available $LiFePO_4$, mixed phosphates and $LiCoO_2$.

3.2.7 Lab-scale Li metal cell testing

The electrochemical stability of poly[(LiM$_{17}$-*r*-PEGM$_{86}$)-*b*-PhEtM$_{131}$] block copolymer was further confirmed by galvanostatic cycling (Fig. 12) in lab-scale cell with a composite $LiFePO_4$-based cathode in the voltage range between 2.5 V and 4 V vs. Li^+/Li (Fig. 12b). The LFP-based electrode was prepared in the form of a catholyte using poly[(LiM$_{17}$-*r*-PEGM$_{86}$)-*b*-PhEtM$_{131}$] block copolymer as an active binder to enhance the interfacial contact between solid polymer electrolyte and electrode active materials. The lab-scale Li/poly[(LiM$_{17}$-*r*-PEGM$_{86}$)-*b*-PhEtM$_{131}$]/$LiFePO_4$ cell was assembled using neat block copolymer as separator without any further treatment of the electrodes or in the absence of any plasticizers/enhancers (e.g., solvents, salts). The electrochemical behavior of the all-solid-state lab-scale cell was investigated by galvanostatic cycling at 70 °C at increasingly high C rates (C/n, n = 20, 10, 5) calculated over the theoretical specific capacity of the LFP active material (170 mAh g^{-1}). The rate capability test performed at different C rates (Fig. 12a) resulted in a specific capacity retention above 95% while moving from C/20 to C/5.

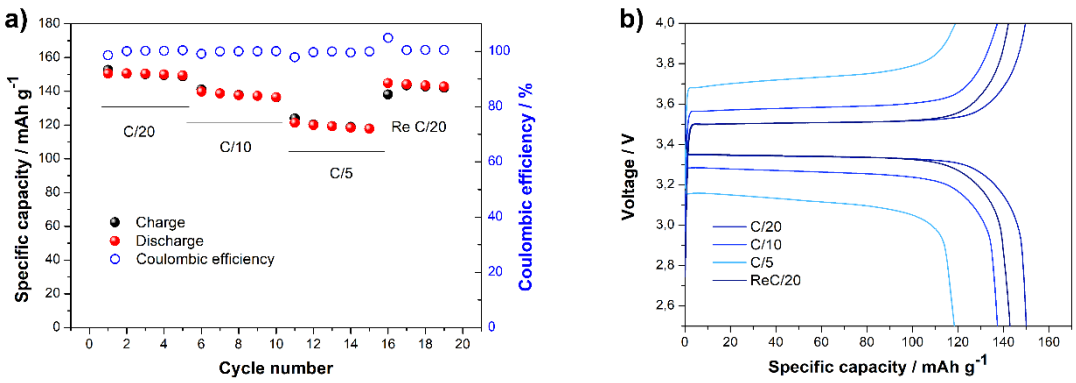

Fig. 12. Galvanostatic cycling behavior of Li/poly[(LiM$_{17}$-*r*-PEGM$_{86}$)-*b*-PhEtM$_{131}$]/LFP solid-state cells at 70 °C. Specific capacity vs. cycle number dependence (a) and corresponding charge/discharge voltage vs. specific capacity profiles at a constant (b) at C/20, C/10 and C/5.

Figure 12b shows clean potential versus specific capacity profiles and typical flat plateaus even upon increasing the current regime, indicating highly reversible and stable single-phase de-/insertion (charge/discharge) mechanism from/in the $LiFePO_4/FePO_4$.

The small overpotential increase (up to ~0.2V at C/5) was likely ascribed to the relatively high complex viscosity of the polyelectrolyte, which limits the mobility of the side chains and the overall Li^+ conduction. The excellent Coulombic efficiency and capacity retention at C/20 current rate after several cycles at higher C rates clearly point out the remarkable electrolyte compatibility with both Li metal and LFP with no electrolyte degradation and/or severe passivation reactions (Fig. 12a). Improved mechanical properties of poly[(LiM_{17}-*r*-$PEGM_{86}$)-*b*-$PhEtM_{131}$] in comparison with poly[LiM_{17}-*r*-$PEGM_{86}$] along with suitable ionic conductivity allowed stable and efficient charge/discharge cycling (> 150 mAh g^{-1}) at the first cycle, which corresponds to >94% of the practical specific capacity (158 mAh g^{-1} at C/20) provided by the commercial LFP used as the active material when cycled with a standard LP30 liquid electrolyte (Fig. 13). Excellent cycling stability and capacity retention were demonstrated even upon prolonged cycling, with coulombic efficiency (CE) values approaching 100% during the whole cycling test, in which the lab-scale Li metal polymer cell was able to deliver 131 mAh g^{-1} after more than 75 cycles with a capacity retention of 87% (Fig. 13).

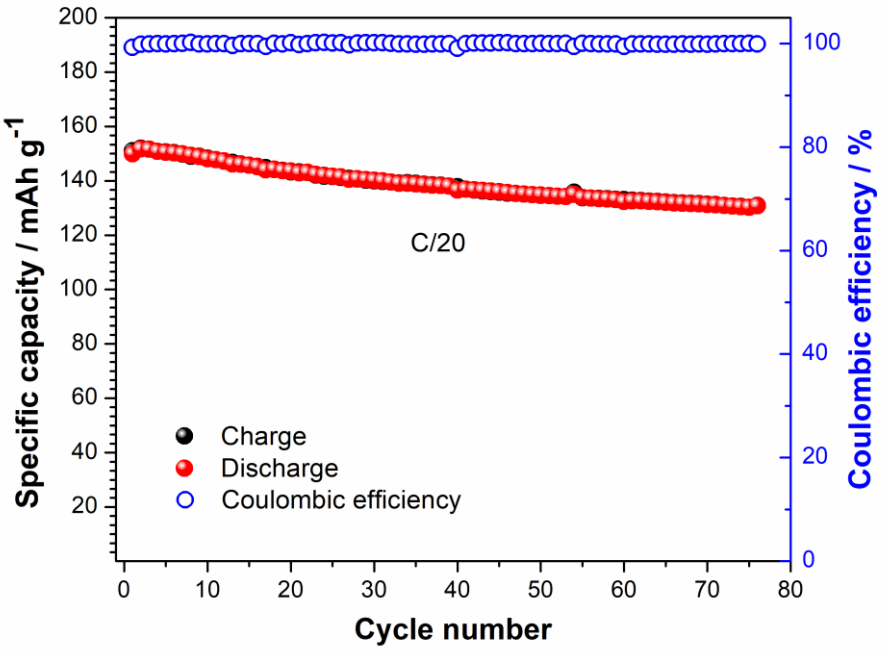

Fig. 13. Galvanostatic cycling behavior of Li/poly[(LiM_{17}-*r*-$PEGM_{86}$)-*b*-$PhEtM_{131}$]/LFP solid-state cells at C/20 and 70 °C.

Overall, this is an excellent result, especially taking into account the active material loading (3.89 mg/cm^2), which is sufficiently high for a truly solid lab-scale polymer electrolyte cell [63] and not too far from standard commercial cells operating with liquid electrolytes [64]. The remarkable electrochemical performance in terms of high-capacity output and capacity retention after more than 75 consecutive charge/discharge cycles at C/20 rate is likely ascribed to the efficient ion transport in the solid polymer electrolyte and the favorable charge transport due to the optimal electrode/electrolyte interface in the cell.

4. Conclusions

In this work, we described the synthesis, thermo-mechanical and chemico-physical properties of novel single-ion conducting block copolymers (A-*b*-B), possessing randomly distributed Li-conducting and ion-solvating segments in the first block (A), which is accompanied by incompatible poly(2-phenylethyl methacrylate) block (B) providing mechanical strength and initiating phase segregation. Such poly[(LiM$_n$-*r*-PEGM$_m$)-*b*-PhEtM$_k$] copolymers were synthesized by segmental RAFT copolymerization, allowing to control the length of both blocks. Thus, a series of nine block copolymers with a range of molecular weights $M_{n(SEC)}$ = 24.3 ÷74.7 kDa ($M_{n(NMR)}$ = 25.8 ÷ 85.9 kDa) and low polydispersity M_w/M_n =1.12 ÷ 1.21 was prepared varying the content of Li^+ cations in A-block (LiM/PEGM ratio) and the ratios between ionic and nonionic blocks (M_A/M_B). The formation of block copolymers was confirmed by comprehensive set of techniques, including NMR and IR spectroscopy, gel permeation chromatography (GPC SEC), thermal mechanical analysis (TMA) and atomic force microscopy (AFM).

AFM images demonstrated two types of morphology: perpendicular hexagonally packed cylinders (HPC) and perpendicular lamellas. Six block copolymers with low molecular weights showed the segregation into HPC morphology and their ionic conductivity was lower in comparison with parent poly[LiM$_n$-*r*-PEGM$_m$] copolymers. The long-range-ordered lamellar morphology with the domains length of 34.1 ÷ 38.7 nm occurred only in high molecular weight block copolymers ($M_{n(NMR)}$ = 74.1 ÷ 85.9 kDa) possessing the ratio between ionic (A) and nonionic blocks (B) lower than two (M_A/M_B ≤2.0) and the ratio of PEGM:LiM equal to 5:1. The ionic conductivity in such

poly[(LiM$_{17}$-*r*-PEGM$_{86}$)-*b*-PhEtM$_{131}$] and poly[(LiM$_{17}$-*r*-PEGM$_{86}$)-*b*-PhEtM$_{194}$] samples (~3.6×10^{-7} S/cm at 25°C) was almost approaching the conductivity of initial ionic A-blocks (4.1×10^{-7} S/cm at 25°C) despite the significant decrease in the concentration of mobile charges. Moreover, these block copolymers showed an improved viscoelastic performance in comparison with parent poly[LiM$_{17}$-*r*-PEGM$_{86}$] copolymer (an enhancement of four orders of magnitude in complex viscosity and up to five orders of magnitude in storage modulus at 25^{o}C). Thus, the ionic conductivity in SICP block copolymers was found to be dependent on their morphology. While cylindrical morphology resulted in the decrease in ionic conductivity, the lamellar samples exhibited conductivity comparable to the parent ionic A-blocks. Such results were attributed to the formation of the nano-sized channels with high concentration of Li cations responsible for conductivity and poly(PhEtM) based phase accountable for toughness.

The proof-of-concept lab-scale truly-solid-state Li-metal cells were assembled with the optimal poly[(LiM$_{17}$-*r*-PEGM$_{86}$)-*b*-PhEtM$_{131}$] block copolymer and LFP-based composite electrode. The Li/poly[(LiM$_{17}$-*r*-PEGM$_{86}$)-*b*-PhEtM$_{131}$]/LiFePO$_4$ cells were studied at 70^{o}C and provided excellent performances in terms of high specific capacity output, stability and reversible cycling at high active material loading for a solid-state system. They were able to deliver 131 mAh g^{-1} after more than 75 cycles at C/20 rate with a capacity retention of 86.67%. The most striking advantages of the suggested approach can be summarized as follows: (1) the possibility to prepare SICP block copolymers with the control over the molecular weights of both blocks; (2) the ability to control both the ionic conductivity and morphology of block copolymers simply varying the PEGM/LiM and ionic/nonionic blocks (M_A/M_B) ratios; (3) the synthesis of solid polymer electrolytes with comparatively high σ (up to 3.8×10^{-7} and 1.0×10^{-5} S/cm at 25 and 70 °C, respectively) and enhanced mechanical properties; (4) the preparation of single ion conductors with high lithium transference number (0.96) and high anodic oxidation stability (4.4 V vs. Li^{+}/Li at 70^{o}C); (5) the assembly of lithium polymer metal batteries capable to deliver comparably large capacities (up to 150 mAh g^{-1} at 70^{o}C) and to reversibly operate at medium current rates (up to C/5). The comprehensive study carried out on novel materials and synthetic approaches enlightens the promising prospects on the use of safe, electrochemically stable singe-ion conducting electrolytes in advanced solid-state Li-metal based battery technologies.

ASSOCIATED CONTENT

Supporting Information

The Supporting Information contains full details on materials and synthesis procedures; tables with the loadings for the synthesis of $(LiM)_n$-*r*-$(PEGM)_m$, poly(PEGM) and poly[(LiM_n-*r*-$PEGM_m$)-*b*-$PhEtM_k$] block copolymers; tables with selected properties of poly[LiM_n-*r*-$PEGM_m$] and poly(PEGM); kinetic plots for PhEtM RAFT polymerization; DSC traces, NMR and IR spectra of poly(PhEtM); AFM images of poly[(LiM_6-*r*-$PEGM_{27}$)-*b*-$PhEtM_{53}$], poly[(LiM_{17}-*r*-$PEGM_{50}$)-*b*-$PhEtM_{82}$], poly[(LiM_{11}-*r*-$PEGM_{54}$)-*b*-$PhEtM_{40}$] and poly[(LiM_{17}-*r*-$PEGM_{86}$)-*b*-$PhEtM_{75}$] films; Li ion transference number (t_{Li}^+) determination and the study of electrochemical stability window (ESW) for poly[(LiM_{17}-*r*-$PEGM_{86}$)-*b*-$PhEtM_{131}$].

Acknowledgements

Synthesis of random poly[$(LiM)_n$-*r*-$(PEGM)_m$] and block poly[(LiM_n-*r*-$PEGM_m$)-*b*-$PhEtM_k$] copolymers as well as the investigation of their ionic conductivity were supported by the Russian Science Foundation (project no. 21-13-00173). Elemental analysis and IR spectroscopy were performed with the financial support from Ministry of Science and Higher Education of the Russian Federation using the equipment of Center for molecular composition studies of INEOS RAS. The financial support for Li-ion transference number, anodic stability and investigation of lab scale Li/copolymer/$LiFePO_4$ cells was in part provided by ENABLES project (http://www.enables-project.eu/) that has received funding from the European Union's Horizon 2020 research and innovation program (project no. 730957). G. Lingua is grateful to the Luxembourg Institute of Science and Technology (LIST) for the partial sponsorship of his visit and work in Materials and Research Technology Department (MRT).

References

[1] J.-M. Tarascon, M. Armand, Issues and challenges facing rechargeable lithium batteries, Nature. 414 (2001) 359–367. https://doi.org/10.1038/35104644.

[2] J.B. Goodenough, Y. Kim, Challenges for Rechargeable Li Batteries, Chem. Mater. 22 (2010) 587–603. https://doi.org/10.1021/cm901452z.
[3] Z. Yang, J. Zhang, M.C.W. Kintner-Meyer, X. Lu, D. Choi, J.P. Lemmon, J. Liu, Electrochemical Energy Storage for Green Grid, Chem. Rev. 111 (2011) 3577–3613. https://doi.org/10.1021/cr100290v.
[4] L. Long, S. Wang, M. Xiao, Y. Meng, Polymer electrolytes for lithium polymer batteries, J. Mater. Chem. A. 4 (2016) 10038–10069. https://doi.org/10.1039/C6TA02621D.
[5] T. Placke, R. Kloepsch, S. Dühnen, M. Winter, Lithium ion, lithium metal, and alternative rechargeable battery technologies: the odyssey for high energy density, J. Solid State Electrochem. 21 (2017) 1939–1964. https://doi.org/10.1007/s10008-017-3610-7.
[6] A. Hammami, N. Raymond, M. Armand, Runaway risk of forming toxic compounds, Nature. 424 (2003) 635–636. https://doi.org/10.1038/424635b.
[7] K. Xu, Nonaqueous Liquid Electrolytes for Lithium-Based Rechargeable Batteries, Chem. Rev. 104 (2004) 4303–4418. https://doi.org/10.1021/cr030203g.
[8] M. Armand, J.-M. Tarascon, Building better batteries, Nature. 451 (2008) 652–657. https://doi.org/10.1038/451652a.
[9] L. Li, S. Li, Y. Lu, Suppression of dendritic lithium growth in lithium metal-based batteries, Chem. Commun. 54 (2018) 6648–6661. https://doi.org/10.1039/C8CC02280A.
[10] D.E. Fenton, J.M. Parker, P.V. Wright, Complexes of alkali metal ions with poly(ethylene oxide), Polymer. 14 (1973) 589. https://doi.org/10.1016/0032-3861(73)90146-8.
[11] V. Di Noto, S. Lavina, G.A. Giffin, E. Negro, B. Scrosati, Polymer electrolytes: Present, past and future, Electrochimica Acta. 57 (2011) 4–13. https://doi.org/10.1016/j.electacta.2011.08.048.
[12] N.S. Schauser, K.J. Harry, D.Y. Parkinson, H. Watanabe, N.P. Balsara, Lithium Dendrite Growth in Glassy and Rubbery Nanostructured Block Copolymer Electrolytes, J. Electrochem. Soc. 162 (2015) A398–A405. https://doi.org/10.1149/2.0511503jes.
[13] H. Zhang, C. Li, M. Piszcz, E. Coya, T. Rojo, L.M. Rodriguez-Martinez, M. Armand, Z. Zhou, Single lithium-ion conducting solid polymer electrolytes: advances and perspectives, Chem. Soc. Rev. 46 (2017) 797–815. https://doi.org/10.1039/C6CS00491A.
[14] M. Forsyth, L. Porcarelli, X. Wang, N. Goujon, D. Mecerreyes, Innovative Electrolytes Based on Ionic Liquids and Polymers for Next-Generation Solid-State Batteries, Acc. Chem. Res. 52 (2019) 686–694. https://doi.org/10.1021/acs.accounts.8b00566.
[15] C. Kirsch, M. Pulst, M.H. Samiullah, P. Ruda, N. Hasan, J. Kressler, 1,2,3-Triazole mediated Li+-ion conductivity in poly(ethylene oxide) based electrolytes, Solid State Ion. 309 (2017) 163–169. https://doi.org/10.1016/j.ssi.2017.07.022.
[16] A. Narita, W. Shibayama, N. Matsumi, H. Ohno, Novel ion conductive matrix via dehydrocoupling polymerization of imidazolium-type ionic liquid and lithium 9-borabicyclo[3,3,1]nonane hydride, Polym. Bull. 57 (2006) 109–114. https://doi.org/10.1007/s00289-006-0527-1.
[17] S. Liang, U.H. Choi, W. Liu, J. Runt, R.H. Colby, Synthesis and Lithium Ion Conduction of Polysiloxane Single-Ion Conductors Containing Novel Weak-

Binding Borates, Chem. Mater. 24 (2012) 2316–2323. https://doi.org/10.1021/cm3005387.
[18] U.H. Choi, S. Liang, M.V. O'Reilly, K.I. Winey, J. Runt, R.H. Colby, Influence of Solvating Plasticizer on Ion Conduction of Polysiloxane Single-Ion Conductors, Macromolecules. 47 (2014) 3145–3153. https://doi.org/10.1021/ma500146v.
[19] F. Ahmed, I. Choi, Md.M. Rahman, H. Jang, T. Ryu, S. Yoon, L. Jin, Y. Jin, W. Kim, Remarkable Conductivity of a Self-Healing Single-Ion Conducting Polymer Electrolyte, Poly(ethylene- *co* -acrylic lithium (fluoro sulfonyl)imide), for All-Solid-State Li-Ion Batteries, ACS Appl. Mater. Interfaces. 11 (2019) 34930–34938. https://doi.org/10.1021/acsami.9b10474.
[20] J. Rolland, E. Poggi, A. Vlad, J.-F. Gohy, Single-ion diblock copolymers for solid-state polymer electrolytes, Polymer. 68 (2015) 344–352. https://doi.org/10.1016/j.polymer.2015.04.056.
[21] S.-W. Ryu, P.E. Trapa, S.C. Olugebefola, J.A. Gonzalez-Leon, D.R. Sadoway, A.M. Mayes, Effect of Counter Ion Placement on Conductivity in Single-Ion Conducting Block Copolymer Electrolytes, J. Electrochem. Soc. 152 (2005) A158–A163. https://doi.org/10.1149/1.1828244.
[22] H. Yuan, J. Luan, Z. Yang, J. Zhang, Y. Wu, Z. Lu, H. Liu, Single Lithium-Ion Conducting Solid Polymer Electrolyte with Superior Electrochemical Stability and Interfacial Compatibility for Solid-State Lithium Metal Batteries, ACS Appl. Mater. Interfaces. 12 (2020) 7249–7256. https://doi.org/10.1021/acsami.9b20436.
[23] K. Matsumoto, T. Endo, Preparation and properties of ionic-liquid-containing poly(ethylene glycol)-based networked polymer films having lithium salt structures, J. Polym. Sci. Part Polym. Chem. 49 (2011) 3582–3587. https://doi.org/10.1002/pola.24795.
[24] R. Meziane, J.-P. Bonnet, M. Courty, K. Djellab, M. Armand, Single-ion polymer electrolytes based on a delocalized polyanion for lithium batteries, Electrochimica Acta. 57 (2011) 14–19. https://doi.org/10.1016/j.electacta.2011.03.074.
[25] R. Bouchet, S. Maria, R. Meziane, A. Aboulaich, L. Lienafa, J.-P. Bonnet, T.N.T. Phan, D. Bertin, D. Gigmes, D. Devaux, R. Denoyel, M. Armand, Single-ion BAB triblock copolymers as highly efficient electrolytes for lithium-metal batteries, Nat. Mater. 12 (2013) 452–457. https://doi.org/10.1038/nmat3602.
[26] S. Feng, D. Shi, F. Liu, L. Zheng, J. Nie, W. Feng, X. Huang, M. Armand, Z. Zhou, Single lithium-ion conducting polymer electrolytes based on poly[(4-styrenesulfonyl)(trifluoromethanesulfonyl)imide] anions, Electrochimica Acta. 93 (2013) 254–263. https://doi.org/10.1016/j.electacta.2013.01.119.
[27] Y. Zhang, C.A. Lim, W. Cai, R. Rohan, G. Xu, Y. Sun, H. Cheng, Design and synthesis of a single ion conducting block copolymer electrolyte with multifunctionality for lithium ion batteries, RSC Adv. 4 (2014) 43857–43864. https://doi.org/10.1039/C4RA08709G.
[28] C. Jangu, A.M. Savage, Z. Zhang, A.R. Schultz, L.A. Madsen, F.L. Beyer, T.E. Long, Sulfonimide-Containing Triblock Copolymers for Improved Conductivity and Mechanical Performance, Macromolecules. 48 (2015) 4520–4528. https://doi.org/10.1021/acs.macromol.5b01009.
[29] P.-F. Cao, B. Li, G. Yang, S. Zhao, J. Townsend, K. Xing, Z. Qiang, K.D. Vogiatzis, A.P. Sokolov, J. Nanda, T. Saito, Elastic Single-Ion Conducting Polymer Electrolytes: Toward a Versatile Approach for Intrinsically Stretchable Functional

Polymers, Macromolecules. 53 (2020) 3591–3601. https://doi.org/10.1021/acs.macromol.9b02683.
[30] Q. Ma, H. Zhang, C. Zhou, L. Zheng, P. Cheng, J. Nie, W. Feng, Y.-S. Hu, H. Li, X. Huang, L. Chen, M. Armand, Z. Zhou, Single Lithium-Ion Conducting Polymer Electrolytes Based on a Super-Delocalized Polyanion, Angew. Chem. Int. Ed. 55 (2016) 2521–2525. https://doi.org/10.1002/anie.201509299.
[31] G. Chen, C. Niu, Y. Chen, W. Shang, Y. Qu, Z. Du, L. Zhao, X. Liao, J. Du, Y. Chen, A single-ion conducting polymer electrolyte based on poly(lithium 4-styrenesulfonate) for high-performance lithium metal batteries, Solid State Ion. 341 (2019) 115048. https://doi.org/10.1016/j.ssi.2019.115048.
[32] K. Matsumoto, T. Endo, Synthesis of networked polymers with lithium counter cations from a difunctional epoxide containing poly(ethylene glycol) and an epoxide monomer carrying a lithium sulfonate salt moiety, J. Polym. Sci. Part Polym. Chem. 48 (2010) 3113–3118. https://doi.org/10.1002/pola.24092.
[33] L. Porcarelli, A.S. Shaplov, M. Salsamendi, J.R. Nair, Y.S. Vygodskii, D. Mecerreyes, C. Gerbaldi, Single-Ion Block Copoly(ionic liquid)s as Electrolytes for All-Solid State Lithium Batteries, ACS Appl. Mater. Interfaces. 8 (2016) 10350–10359. https://doi.org/10.1021/acsami.6b01973.
[34] L. Porcarelli, M.A. Aboudzadeh, L. Rubatat, J.R. Nair, A.S. Shaplov, C. Gerbaldi, D. Mecerreyes, Single-ion triblock copolymer electrolytes based on poly(ethylene oxide) and methacrylic sulfonamide blocks for lithium metal batteries, J. Power Sources. 364 (2017) 191–199. https://doi.org/10.1016/j.jpowsour.2017.08.023.
[35] L. Porcarelli, K. Manojkumar, H. Sardon, O. Llorente, A.S. Shaplov, K. Vijayakrishna, C. Gerbaldi, D. Mecerreyes, Single Ion Conducting Polymer Electrolytes Based On Versatile Polyurethanes, Electrochimica Acta. 241 (2017) 526–534. https://doi.org/10.1016/j.electacta.2017.04.132.
[36] L. Porcarelli, P.S. Vlasov, D.O. Ponkratov, E.I. Lozinskaya, D.Y. Antonov, J.R. Nair, C. Gerbaldi, D. Mecerreyes, A.S. Shaplov, Design of ionic liquid like monomers towards easy-accessible single-ion conducting polymer electrolytes, Eur. Polym. J. 107 (2018) 218–228. https://doi.org/10.1016/j.eurpolymj.2018.08.014.
[37] E.I. Lozinskaya, M. Cotessat, A.V. Shmalko, D.O. Ponkratov, L.V. Gumileva, I.B. Sivaev, A.S. Shaplov, Expanding the chemistry of single-ion conducting poly(ionic liquid)s with polyhedral boron anions, Polym. Int. 68 (2019) 1570–1579. https://doi.org/10.1002/pi.5878.
[38] J. Zhu, Z. Zhang, S. Zhao, A.S. Westover, I. Belharouak, P. Cao, Single-Ion Conducting Polymer Electrolytes for Solid-State Lithium–Metal Batteries: Design, Performance, and Challenges, Adv. Energy Mater. 11 (2021) 2003836. https://doi.org/10.1002/aenm.202003836.
[39] G.G. Eshetu, D. Mecerreyes, M. Forsyth, H. Zhang, M. Armand, Polymeric ionic liquids for lithium-based rechargeable batteries, Mol. Syst. Des. Eng. 4 (2019) 294–309. https://doi.org/10.1039/C8ME00103K.
[40] D.R. Sadoway, Block and graft copolymer electrolytes for high-performance, solid-state, lithium batteries, J. Power Sources. 129 (2004) 1–3. https://doi.org/10.1016/j.jpowsour.2003.11.016.
[41] A.S. Shaplov, R. Marcilla, D. Mecerreyes, Recent Advances in Innovative Polymer Electrolytes based on Poly(ionic liquid)s, Electrochim Acta. 175 (2015) 18–34. https://doi.org/10.1016/j.electacta.2015.03.038.

[42] Y. Ye, J.-H. Choi, K.I. Winey, Y.A. Elabd, Polymerized Ionic Liquid Block and Random Copolymers: Effect of Weak Microphase Separation on Ion Transport, Macromolecules. 45 (2012) 7027–7035. https://doi.org/10.1021/ma301036b.
[43] J.-H. Choi, Y. Ye, Y.A. Elabd, K.I. Winey, Network Structure and Strong Microphase Separation for High Ion Conductivity in Polymerized Ionic Liquid Block Copolymers, Macromolecules. 46 (2013) 5290–5300. https://doi.org/10.1021/ma400562a.
[44] K.M. Meek, Y.A. Elabd, Polymerized ionic liquid block copolymers for electrochemical energy, J Mater Chem A. 3 (2015) 24187–24194. https://doi.org/10.1039/C5TA07170D.
[45] J.R. Nykaza, Y. Ye, R.L. Nelson, A.C. Jackson, F.L. Beyer, E.M. Davis, K. Page, S. Sharick, K.I. Winey, Y.A. Elabd, Polymerized ionic liquid diblock copolymers: impact of water/ion clustering on ion conductivity, Soft Matter. 12 (2016) 1133–1144. https://doi.org/10.1039/C5SM02053K.
[46] J.R. Nykaza, Y. Ye, Y.A. Elabd, Polymerized ionic liquid diblock copolymers with long alkyl side-chain length, Polymer. 55 (2014) 3360–3369. https://doi.org/10.1016/j.polymer.2014.04.003.
[47] V.F. Scalfani, E.F. Wiesenauer, J.R. Ekblad, J.P. Edwards, D.L. Gin, T.S. Bailey, Morphological Phase Behavior of Poly(RTIL)-Containing Diblock Copolymer Melts, Macromolecules. 45 (2012) 4262–4276. https://doi.org/10.1021/ma300328u.
[48] S. Inceoglu, A.A. Rojas, D. Devaux, X.C. Chen, G.M. Stone, N.P. Balsara, Morphology–Conductivity Relationship of Single-Ion-Conducting Block Copolymer Electrolytes for Lithium Batteries, ACS Macro Lett. 3 (2014) 510–514. https://doi.org/10.1021/mz5001948.
[49] A.A. Rojas, S. Inceoglu, N.G. Mackay, J.L. Thelen, D. Devaux, G.M. Stone, N.P. Balsara, Effect of Lithium-Ion Concentration on Morphology and Ion Transport in Single-Ion-Conducting Block Copolymer Electrolytes, Macromolecules. 48 (2015) 6589–6595. https://doi.org/10.1021/acs.macromol.5b01193.
[50] J.L. Thelen, S. Inceoglu, N.R. Venkatesan, N.G. Mackay, N.P. Balsara, Relationship between Ion Dissociation, Melt Morphology, and Electrochemical Performance of Lithium and Magnesium Single-Ion Conducting Block Copolymers, Macromolecules. 49 (2016) 9139–9147. https://doi.org/10.1021/acs.macromol.6b01886.
[51] D. Devaux, L. Liénafa, E. Beaudoin, S. Maria, T.N.T. Phan, D. Gigmes, E. Giroud, P. Davidson, R. Bouchet, Comparison of single-ion-conductor block-copolymer electrolytes with Polystyrene- TFSI and Polymethacrylate- TFSI structural blocks, Electrochimica Acta. 269 (2018) 250–261. https://doi.org/10.1016/j.electacta.2018.02.142.
[52] G. Lingua, P. Grysan, P.S. Vlasov, P. Verge, A.S. Shaplov, C. Gerbaldi, Unique Carbonate-Based Single Ion Conducting Block Copolymers Enabling High-Voltage, All-Solid-State Lithium Metal Batteries, Macromolecules. 54 (2021) 6911–6924. https://doi.org/10.1021/acs.macromol.1c00981.
[53] Y. Mai, A. Eisenberg, Self-assembly of block copolymers, Chem. Soc. Rev. 41 (2012) 5969. https://doi.org/10.1039/c2cs35115c.
[54] R.L. Weber, Y. Ye, A.L. Schmitt, S.M. Banik, Y.A. Elabd, M.K. Mahanthappa, Effect of Nanoscale Morphology on the Conductivity of Polymerized Ionic Liquid

Block Copolymers, Macromolecules. 44 (2011) 5727–5735. https://doi.org/10.1021/ma201067h.
[55] L. Li, S. Li, Y. Lu, Suppression of dendritic lithium growth in lithium metal-based batteries, Chem. Commun. 54 (2018) 6648–6661. https://doi.org/10.1039/c8cc02280a.
[56] J. Liu, J. Zhou, M. Wang, C. Niu, T. Qian, C. Yan, A functional-gradient-structured ultrahigh modulus solid polymer electrolyte for all-solid-state lithium metal batteries, J. Mater. Chem. A. 7 (2019) 24477–24485. https://doi.org/10.1039/c9ta07876b.
[57] J. Evans, C.A. Vincent, P.G. Bruce, Electrochemical measurement of transference numbers in polymer electrolytes, Polymer. 28 (1987) 2324–2328. https://doi.org/10.1016/0032-3861(87)90394-6.
[58] K.M. Abraham, Z. Jiang, B. Carroll, Highly Conductive PEO-like Polymer Electrolytes, Chem. Mater. 9 (1997) 1978–1988. https://doi.org/10.1021/cm970075a.
[59] L. Yue, J. Ma, J. Zhang, J. Zhao, S. Dong, Z. Liu, G. Cui, L. Chen, All solid-state polymer electrolytes for high-performance lithium ion batteries, Energy Storage Mater. 5 (2016) 139–164. https://doi.org/10.1016/j.ensm.2016.07.003.
[60] I. Osada, H. de Vries, B. Scrosati, S. Passerini, Ionic-Liquid-Based Polymer Electrolytes for Battery Applications, Angew. Chem. Int. Ed. 55 (2016) 500–513. https://doi.org/10.1002/anie.201504971.
[61] M.J. Park, I. Choi, J. Hong, O. Kim, Polymer electrolytes integrated with ionic liquids for future electrochemical devices, J. Appl. Polym. Sci. 129 (2013) 2363–2376. https://doi.org/10.1002/app.39064.
[62] X. Yang, M. Jiang, X. Gao, D. Bao, Q. Sun, N. Holmes, H. Duan, S. Mukherjee, K. Adair, C. Zhao, J. Liang, W. Li, J. Li, Y. Liu, H. Huang, L. Zhang, S. Lu, Q. Lu, R. Li, C.V. Singh, X. Sun, Determining the limiting factor of the electrochemical stability window for PEO-based solid polymer electrolytes: main chain or terminal –OH group?, Energy Environ. Sci. 13 (2020) 1318–1325. https://doi.org/10.1039/D0EE00342E.
[63] E. Quartarone, P. Mustarelli, Electrolytes for solid-state lithium rechargeable batteries: recent advances and perspectives, Chem. Soc. Rev. 40 (2011) 2525. https://doi.org/10.1039/c0cs00081g.
[64] R. Moshtev, B. Johnson, State of the art of commercial Li ion batteries, J. Power Sources. 91 (2000) 86–91. https://doi.org/10.1016/S0378-7753(00)00458-4.